Investigating Moisture Gradient-Induced Warpage of Wood Veneers

Kerrigan A. Strong

Thesis submitted to the faculty of the Virginia Polytechnic Institute and State University

in partial fulfillment of the requirements for the degree of

Master of Science

In

Forest Products

Joseph Loferski, Chairman

Daniel Hindman

James Hanna

24 June 2021

Blacksburg, VA

Keywords: Warpage, Moisture, Moisture induction, Moisture gradient, Deformation measurements, Wood, Veneers, Three-dimensional scanning, Curvature comb analysis

Investigating Moisture Gradient-Induced Warpage of Veneers

by

Kerrigan A. Strong

Abstract

Flatness of wood composite panels, such as Laminated Veneer Lumber, is often difficult to control during the manufacturing process. Out-of-plane deformation, or warpage, of wood veneers caused by changes in moisture content affects the ability to press flat panels. To understand wood panel warpage, experimental methods are developed to create and measure moisture-induced deformation of wood veneers on five species of various thicknesses. Three moisture induction methods are investigated and evaluated to determine the increase in moisture content. Experiments are developed to produce moisture gradients of two concentrations in the veneers to examine the effect on warpage behavior. Additionally, the surface area of applied moisture and veneer thickness is also investigated.

Three-dimensional scanning technology is used to measure warpage of veneers. A procedure using a structured-light scanner is developed to analyze the surface curvatures to observe the effect of moisture-induced warpage. After moisture-induction treatment of the veneer, surface deformation data is measured using the scanner and the data is converted into a 3D solid body model that is used for curvature comb analysis.

The results show that curvature comb analysis can be used to analyze the geometry of moisture-induce warpage. The method can be used to analyze the effect of moisture gradient variables on warpage behavior including concentration, veneer thickness, and surface area. The experimental methods developed can be used by future researchers to validate theoretical warpage prediction models.

Investigating Moisture Gradient-Induced Warpage of Veneers

by

Kerrigan A. Strong

General Audience Abstract

Flatness of wood composite panels, such as Laminated Veneer Lumber, is often difficult to control during the manufacturing process. Warpage of wood veneers is caused by changes in moisture content affecting manufacturers' ability to press flat panels. To understand wood panel warpage, experimental methods are developed to create and measure moisture-induced warpage of wood veneers on five species of various thicknesses. Three moisture induction methods are investigated and evaluated to determine the increase in moisture content. Experiments are developed to produce moisture gradients of two concentrations in the veneers to examine the effect on warpage behavior. Additionally, the surface area of applied moisture and veneer thickness is also investigated.

Three-dimensional scanning technology is used to measure warpage of veneers. A procedure is developed to analyze the surface curvatures to observe the effect of moisture-induced warpage. After moisture-induction treatment of the veneer, surface deformation data is measured and converted into a 3D solid body model that is used to analyze curvature.

The results show that moisture induction methods used to induce warpage can experience different geometries to analyze a veneer's curvature. The methods can be used to analyze warpage behavior of veneers by future researchers to validate warpage prediction model.

Acknowledgements

I would like to dedicate this section to the great minds and incredible people who have helped me along the way. First, I would like to thank my family for their love and support throughout my 18 years of formal education. Also, thank you to the great friends who have always pushed me to do my best, especially my classmate Angela Rara. I wouldn't be where I am today without my family and friends as my support system.

I would like to thank Dr. Joseph Loferski for taking me on as a graduate student. Additionally, thank you to my committee, Dr. Daniel Hindman and Dr. James Hanna, for your help and support during my Masters program. It was an honor to be able to have such intelligent mentors throughout completion of this program.

Additionally, I would like to thank the incredible female mentors I had throughout college. I am grateful to Linda Caudill, former managing director of the Wood Based Composites Center, for the endless pep talks and motivation throughout my program. To my former professor, Dr. Audrey Zink-Sharp, thank you for igniting my passion for wood science and always pushing me to do my best.

This project was conducted for the Wood Based Composites Center, a National Science Foundation Industry-University Cooperative Research Center. This material is based upon work supported by the National Science Foundation under Grant No.16245367. Any opinions, findings, and conclusions or recommendations expressed in this material are those of the author and do not necessarily reflect the views of the National Science Foundation.

Table of Contents

List of Figures

List of Tables

1.0 Introduction

In today's engineered wood products industry, it is imperative to produce quality products as quickly and efficiently as possible. During the past century, the use of wood-composite products, such as plywood and LVL, has revolutionized the residential construction industry. Large, flat panels, such as plywood, are used for sheathing of walls, floors, and roofs. Laminated veneer lumber is manufactured from large panels which are cut to size for use as beams, joists, and headers. An advantage of composite products are the uniform characteristics and predictable in-service performance behavior (USDA 2010).

As the demand for wood-composite products increased, so did the need for large-scale manufacturing endeavors. According to the USDA, the forest products industry generates over $200 billion in the United States annually (2021). According to Grand View Research, the industry has an expected compound annual growth rate of 6.9% from 2020 to 2027 (2020).

Manufacturers of wood products must address a variety of issues to produce quality products because of wood's natural variability and hygroscopic properties. Warpage is a large concern for manufacturers "because it often cannot be corrected once it has occurred," wasting thousands of dollars to the industry in unusable products every year (Suchsland and McNatt 1986).

The warpage of wood-based products is caused by moisture content changes during manufacture or changes in environmental conditions in-service. Panel warpage is defined as out-of-plane deformation from a plane. For engineered wood panels, warpage can occur during manufacture and/or during "…the cooling phase after hot-pressing, while in storage, or during application" (Wood 2019). The conditions maintained during manufacturing processes directly affects the quality of a final product.

An important concern for engineered wood panel manufacturers, such as LVL, is the out-of-plane deformation, or warpage, resulting from moisture content (MC) changes during the manufacturing process. A theoretical model (Wood 2019), (Wood and Hanna 2020) was developed to predict warped geometries in anisotropic plates caused by moisture content changes. Inspired by the model, the current project develops methods to create moisture gradients in wood veneers and to measure the subsequent warpage behavior for future research on dimensional stability.

1.1 Goals and Objectives

The goal of this project is to develop methods to create and quantify moisture-induced warpage of wood panels. The objectives of this project are:

1) To develop moisture induction methods to produce shape changes caused by moisture gradients of known magnitude on wood veneers.
2) To investigate and develop methods to measure moisture-induced deformation of warped veneer specimens.

1.2 Project Scope

This project investigates the warpage behavior of veneers subjected to controlled moisture induction techniques applied simultaneously to top and bottom surfaces of a specimen. Moisture gradients are created using a combination of the wetting methods across the surface of a veneer. Two moisture gradient concentrations are investigated to determine the effect on warpage behavior. Five veneer species are used: 1) southern yellow pine (*Pinus spp.)*, 2) Douglas-fir (*Pseudotsuga menziesii*), 3) yellow-poplar (*Liriodendron tulipifera*), 4) red oak

(*Quercus spp*.), and 5) hickory (*Carya spp.*). The three variables explored for their effect on warpage behavior are: 1) veneer thickness, 2) moisture gradient concentration and 3) the surface area of applied gradient.

1.3 Overview

A review of background information and relevant literature pertaining to wood material properties, constitutive laws, studies on wood panel deformation and techniques to measure deformation is presented in Chapter 2. Chapter 3 addresses research objective one, including development of moisture induction methods, evaluation of moisture content measurement methods, and creating moisture gradients for use in the next objective. Results and discussion for the first objective are also included.

Chapter 4 addresses the second objective, including the investigation and development of methods to measure moisture-induced deformation of warped veneer specimens. Topics include qualitative observation of moisture-induced warpage methods, development of the three-dimensional (3D) scanning procedure, and the results and discussion of the warpage experiments.

Chapter 5 provides the summary and conclusions of the project as well a discussion of limitations and suggestions for future research. The references used in this project are recorded in Chapter 6. Finally, the appendix is in Chapter 7 is presented. The data and t-test output from the warpage experiments are reported in the appendix.

2.0 Background and Literature Review

A literature review on the deformation of wood composites is conducted to understand the extent of this problem within the industry as well as understand why wood composites behave the way they do under certain environmental conditions; specifically, changes in moisture content. A review of composite materials with an emphasis on wood-based products is conducted. To follow, properties and mechanics of wood as they relate to warpage are discussed.

Next, studies conducted on the warpage of wood-based materials will be investigated. Techniques to measure subsequent deformation used in warpage experiments and beyond is also discussed in this review. Upon completion of reviewing relevant literature, background knowledge is acquired for designing this experiment based on past works.

2.1 Wood as a Material

Throughout history, wood, as the natural resource obtained from trees, has been utilized to meet basic human needs and beyond. Initially, as it was abundant and readily available, trees were easy to machine into raw material with the use of simple tools. Additionally, wood also proved to provide considerable strength and thermal insulation properties (Lang 1993) which perpetuated its desirability for use. Whether it be for transportation, shelter, or as a source of heat and energy, the numerous applications humans have implemented has established wood as one of the most versatile renewable materials available.

The use of wood for shelter has adapted over the years. Initially, large-diameter roundwood logs were used to create heavy-timber, log cabin-style dwellings. To maximize material efficiency, roundwood was machined on four sides into a prismatic shape to form the wood product known as dimensional lumber. From this development, platform-frame style housing was introduced, and the light frame residential construction industry took off.

During the 20th century, the demand for wood for the residential construction industry increased exponentially as new ways to utilize the raw material were being developed. The first structural plywood product was manufactured at the beginning of that century, slowly gaining industrial and commercial acceptance. It was only after World War II that plywood officially started replacing dimensional lumber as the main material used for sheathing applications (Lang 1993). The utilization of composite materials, like wood-based panel products, has helped rationalize using less material to create a product for structural applications where high strength- and stiffness-to-weight ratios are necessary.

Engineered wood and wood-based panel products often have better characteristics than their constituent material, solid wood. With the development of a composite form of wood material, or an engineered wood product, examples of material properties that improve by fabricating composites include strength, stiffness, wear/corrosion resistance, fatigue life, temperature dependent behaviors, thermal insulation or conductivity, and acoustical insulation. In addition, composite fabrication can even improve the material's appearance (Jones 1975).

When fabricating laminated wood-based composites, the laminate product is made from stacking individual laminae, which is the flatwise arrangement of unidirectional fibers. The fibers serve as the main load-carrying and reinforcing agent and defines the principal material direction. The laminae are stacked – sometimes rotated at alternating orientations to increase the strength and stiffness of the panel – and then using an adhesive bonding agent, the panels are laminated to form an inhomogeneous composite material (Shmulsky and Jones 2011). Figure

2.1.1 shows an example of a panel that rotates the fiber direction for each lamina where the grain direction is indicated by arrowheads.

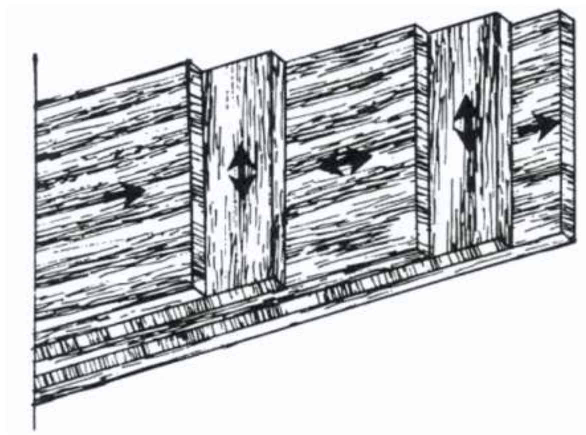

Figure 2.1.1: Layup for a plywood panel demonstrating cross-grain direction (Sellers 1985).

In Figure 2.1.1, the individual layers, or laminae, for this composite are wood veneers. In laminated wood-based panel composites, veneers are the laminae most often used. The manufacturer strategically orients each panel's fiber direction for each individual lamina, rotating the veneers 90° with each addition of another layer. By utilizing the process of lamination, engineers can tailor the directional dependence of a material's properties to match the loading environment for a structural element (Bodig and Jayne 1982).

Since the beginning of its exploitation, wood has been revered for its variety of unique uses. As a building material, wood is considered one of the easiest and simplest products that can be used (Shumlsky and Jones 2011). Wood is easily machinable and can be cut quickly into the intended design for end use. In combination with easily incorporated fasteners, wood can be used for a multitude of purposes. Due to its readily available, value-added nature, wood has proven to be one of the world's most popular materials.

2.2 Wood Properties

Following the establishment of wood as a versatile product, the specific properties and behaviors that influence the material characteristics of this biomaterial are explored. Wood, as a natural material, has a unique relationship with water and their interactions on a micro- and macroscopic level are discussed in textbooks (Bodig and Jayne 1982), (Shumlsky and Jones 2011) and the Wood Handbook (USDA 2010).

Wood is a material that has strength and is resistant to deformation. The mechanical properties of wood are used to define the inherent characteristics of the material. Strength is the ability for a material to carry an applied force or load. A material's resistance to deformation, or stiffness, describes how much an applied load will distort, or warp, the material. Mechanical properties, such as strength and stiffness, are important when determining a product's use in structural applications (Shumlsky and Jones 2011).

To fully understand the extent of wood's properties, the material's microscopic structure is investigated. Inside of a tree, the cellular structure of wood, or xylem, is comprised of a network of intersecting vertical and horizontal cells. The wood cells oriented parallel to the tree stem are mainly elongated, open and tapered cells that transport water and nutrients longitudinally throughout the tree. The cells perpendicular to the long axis of the tree stem are radial, or ray, cells. Extending from the tree's center to outer bark, ray cells provide horizontal transport of fluids. The formation of wood cell structure is a naturally occurring, biological process that is variable due to many different environmental and ecological factors that affects the cellular structure's growth and formation.

The inhomogeneous cellular structure of xylem is a unique characteristic of wood that significantly affects material properties. Depending on the direction of an externally applied force, the resultant reactions within the body vary among a mutually perpendicular, three-dimensional plane. When properties are a function of orientation at a point within the body, the material is considered orthotropic. To contrast, homogeneous materials like some plastics, metal, and concrete are considered isotropic because they have a uniform composition and experience the same material properties in all directions (Shumlsky and Jones 2011).

To describe wood's orthotropy, the three mutually perpendicular planes of interest are defined. A cut made perpendicularly to the tree's principal, or longitudinal, axis exposes the cross-sectional surface. A cut made tangent to the growth rings exposes the tangential surface and one made in the radial longitudinal direction shows the radial surface. The surfaces are used to describe wood anatomy whereas the three principal directions are used to describe wood mechanics (Bodig and Jayne 1982). The three mutually perpendicular directions of wood are illustrated in Figure 2.2.1.

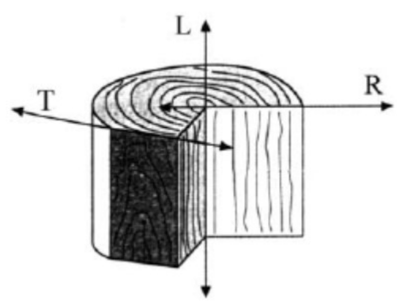

Figure 2.2.1: The three orthotropic directions (tangential, longitudinal, and radial) on a section of a round wood stem (Eyma, Méausoone, and Martin 2001).

Water is a necessary constituent for tree growth. In living xylem, water makes up over half of the wet or "green" weight. As logs and other products are processed from felled trees, moisture from the now dead xylem is lost to the surrounding atmosphere. Drying continues throughout production although some water remains retained within the cell wall's structure (Shmulsky and Jones 2011). Due to its ability to exchange moisture with the surrounding environment, wood is considered hygroscopic. Moisture exchange between wood and air is based on the temperature and relative humidity (RH) of the air and the amount of water within wood (USDA 2010).

Moisture exists in wood cells as either free water (liquid or water vapor in cell pores and lumen) or bound water (moisture retained in cell wall by intermolecular forces). Free water is the first water to leave wood cells during drying. At the point when all the free water has evaporated from cell cavities into the atmosphere, only bound water exists, and the fiber saturation point (FSP) is reached. Below the FSP, the moisture in wood cells is affected by relative humidity and the surrounding air's temperature, causing gradual, short-term moisture fluctuations. Above this point, physical and mechanical properties no longer change as a function of moisture due to the presence of free water (USDA 2010).

Moisture content (MC) is used to describe the amount of water in wood or wood products. This term, expressed as a percentage, is obtained by determining the ratio of water in wood to wood's oven dry weight, or its weight at 0% moisture content. The most reliable method to determine a sample's water weight is by measuring the wet weight, drying the sample in a laboratory oven at 103°C for 24 hours to remove all bound water, and finally, by taking the difference of the sample's wet weight against its oven dry weight. This method is known as the oven-dry gravimetric moisture content determination used in ASTM D4442-20 and is presented in Equation 1 (American Society for Testing and Materials 2020) .

$$percent\ MC = \left(\frac{weight\ with\ water - oven\ dry\ weight}{oven\ dry\ weight}\right) x100 \qquad [1]$$

The FSP for wood averages around 30% moisture content. Wood from freshly cut trees has a moisture content varying from 30% to over 200% (USDA 2010). The moisture content of green wood varies by species and within a tree stem. Once wood is dried below FSP, the free, liquid water in the cell cavities is permanently removed and only bound water remains. Only direct contact with liquid water can cause the increase of moisture content above the FSP (Suchsland 2004). Depending on RH, the average moisture content for wood in normal use varies between 8-25%.

If wood's moisture content falls out of range the atmospheric condition's equilibrium moisture content (EMC), resulting from changes in environmental temperature and relative humidity, water passes through wood cell walls into the air or moisture from the air enters wood cells to achieve equilibrium with its surrounding environment. When moisture movement occurs, the cell wall will shrink or swell in response causing dimensional changes (Suchsland 2004).

Wood is considered dimensionally stable if the moisture content is greater than the fiber saturation point. This is due to saturation of the wood cell with free water, eliminating any further adsorption or desorption. Below FSP, the dimensional stability of wood is affected by the shrinkage and swelling of the wood cells with changing moisture content and thermal expansion due to water desorption and absorption. This occurs when there are changes in environmental conditions or moisture differentials.

The movement of water in wood is a quantifiable mechanism. The relationship between the EMC and RH at a constant temperature is defined by sorption isotherms. A desorption isotherm is determined by bringing originally wet wood to equilibrium by lowering RH. A resorption, or adsorption, isotherm is determined in the opposite manner. Beginning with dry wood, RH is increased. The graphical representation of the sorption isotherm relationships is seen in Figure 2.2.2.

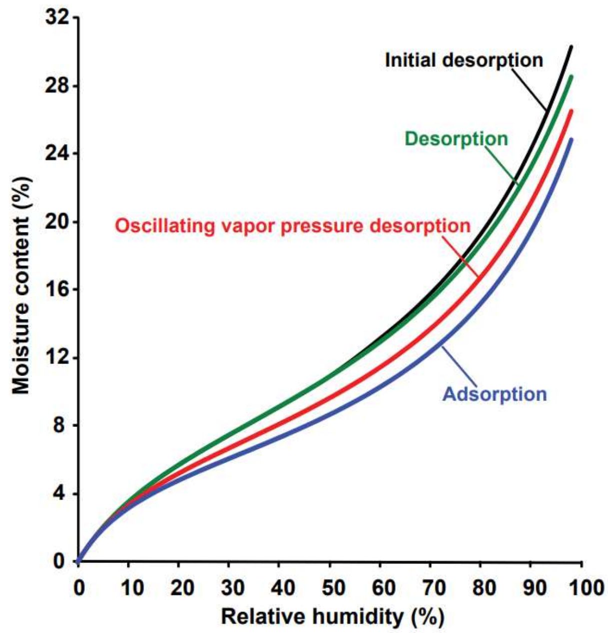

Figure 2.2.2: Sorption isotherms showing the relationship between RH and MC (USDA 2010).

In Figure 2.2.2, it is noted that for the same RH value, MC of adsorption is less than the MC of desorption. When wood dries from its initial green condition to below the FSP, this isotherm is the initial desorption, and its EMC is the greater than all subsequent desorption. The ratio of adsorption EMC to desorption EMC is variable by species, RH, and temperature. Near room temperature (68-72°F), the approximate ratio is 0.8 (USDA 2010).

The difference between the adsorption and desorption curves is a phenomenon known as hysteresis, or the lag effect, and is commonly exhibited in hygroscopic materials (Shmulsky and Jones 2011). Oscillating vapor pressure desorption is used to represent conditions between adsorption and desorption and is used when the direction of sorption is unknown (USDA 2010).

Wood products exposed to liquid water while in service is a concern. If wood contacts liquid water, rapid changes in moisture content result as compared to slower changes associated with water vapor sorption. Liquid water absorption can increase wood's moisture content past the fiber saturation point and can continue until maximum moisture content is reached. The rate of liquid water sorption depends on a variety of factors, including wood species. Liquid sorption is greatest in the longitudinal direction due to the interaction between capillary action and air-water surface tension, creating a pressure gradient that draws water up the cells' lumina (USDA 2010).

Moisture in wood below the FSP causes dimensional changes to individual cells and the overall structure. The volume of the cell wall is based on the amount of bound water and as moisture is gained, the wood swells, and when moisture is lost, the wood shrinks (USDA 2010). Due to wood's orthotropy, the magnitude of dimensional changes caused by moisture differs based on material direction. When considering the three mutually perpendicular directions, warpage occurs greatest tangentially (in the direction of growth rings) and approximately half as much radially, or across the rings. Only a minimal amount of dimensional change is experienced longitudinally, or parallel to the grain direction (USDA 2010).

Wood's hygroscopic nature of exchanging moisture with its surrounding atmosphere influences wood properties and performance (USDA 2010). In all wood-based products, the amount of water in cell walls affects physical and mechanical properties, dimensional stability, and even resistance to biological degradation (Shmulsky and Jones 2011).

In addition to dimensional changes, dry wood results in physical property changes. One example is the increase in strength as wood becomes drier. As wood dries from its green moisture content, the compression strength is doubled. The tensile strength is strongest between 6-12% moisture content (Puuinfo, n.d.).

2.2.1 Constitutive Laws

To understand why wood warps, it is important to explore wood's mechanics and the relationships between stress, strain, and deformation on and within a wood product. The mechanical properties of wood are discussed in textbooks (Bodig and Jayne 1982), (Suchland 2004), and (Shumulsky and Jones 2011). The effect of wood's elastic properties on moisture-induced deformation and the warpage behavior of wood composites will be discussed for their relevancy to this project.

Wood is a solid, yet deformable body. When a compression load is applied, small, compressive deformation results. Increasing the load causes an increase in deformation. Due to wood's orthotropic nature, various relationships exist between an applied force and resultant. For example, a solid piece of lumber is more resistant to deformation in its longitudinal direction than its radial and tangential (Suchsland 2004).

A material's resistance to deformation is called stiffness and is considered a major material property. Because of wood's stiffness, the deformation it experiences can be completely recoverable, up to a point.

Recovery occurs when the externally applied load is removed before the point of unrecoverable deformation is reached. At this critical point, wood is unable to withstand increasing load as irreversible damage has occurred to the individual wood cells. Outlined by the theory of elasticity, a material that has completely recoverable deformation is considered to have ideal elastic behavior. However, no material is perfectly elastic, only experiencing approximately elastic behavior.

The force-deformation relationship and the recoverability of wood based on its elastic behavior is variable. In addition to material stiffness, the ability for wood to recover after loading is affected the following factors: changes in moisture content and temperature, loading rates, loading orientation in relation to symmetry axes, and the amount of deformation that occurs (Bodig and Jayne 1982). When considering the approximately elastic behavior of wood, the relationships specifically pertaining to changes in moisture and the recoverability of deformation will be important to understand for this project.

Robert Hooke (1635-1703) is the scientist to attribute the inception of the modern theories of elasticity. Beginning in 1678, he conducted experiments with wood and other biological materials. By utilizing elastic materials, he determined proportionality laws of force and displacement. He describes the relationship between springy bodies and the concept later known as strain as: “the power of any spring is in the same proportion with the tension there of.” (Bodig and Jayne 1982).

From this determination, it is concluded that one degree of a force, whether a push or pull, will induce one degree of an effect, occurring in a proportional manner. However, Hooke’s experimentation lacked the distinction between elastic and unrecoverable, plastic deformation. In addition, there was no inclusion of the breaking point for a material as a limit to this law. Time dependence and deformation permeance was also ignored (Bodig and Jayne 1982).

The spring model described the behavior of perfectly elastic solids. If the relationship between deformation and applied load is linear, this would be an example of the proportional relationship for perfectly elastic solids that Hooke described. The spring model Hooke determined was used to express this perfectly elastic and proportional behavior. It can also be used to predict and approximate material properties. This is attributed to the fact every material, including different wood species, has its own spring constant, k, which is seen in the force-displacement relationship equation of a linear elastic spring:

$$P = k\Delta \qquad [2]$$

In this first equation, the externally applied force is represented by P and resultant displacement is Δ. Up to a point, wood behaves elastically as the relationship between deformation and applied force is linear. Wood is said to exhibit elastic-plastic behavior, meaning it is elastic up to a point (proportional limit) and then the wood cells start to become damaged and ultimately fail. The relationships of a perfectly elastic material (A) and one that is elastic-plastic (B) is shown in Figure 2.2.3.

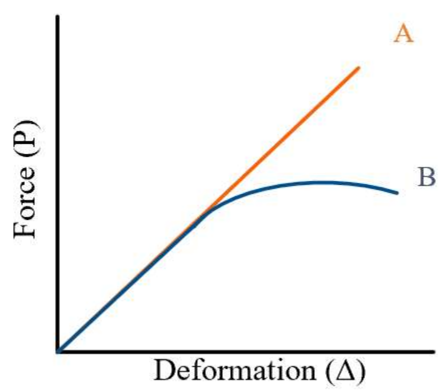

Figure 2.2.3: Graphical representation of the force-deformation relationship of perfectly elastic (A) and elastic-plastic (B) behavior.

In the 1680's, scientist Edme Mariotte used the elastic theories described by Hooke to determine the behavior of materials. Confirming Hooke's determination of the proportional relationship between elongation, or deformation, to the forces applied, Mariotte also noticed failure once elongation surpassed a certain limit. By using the length of the sample, l, and its cross-sectional load contact area, A, a better determination for describing elastic behavior was made that was not included in the spring model [Equation 2]. Using these newfound relationships and the derived spring model equation, Mariotte came up with an equation to describe the concepts of normal stress and normal strain:

$$\frac{P}{A} = \frac{kl}{A}\frac{\Delta l}{l} \qquad [3]$$

From this equation, new material properties, stress and strain, are introduced. A normalized stress load, σ, is defined as the distributed force, P, per unit area, A, on an object.

$$\frac{P}{A} = \sigma \qquad [4]$$

Normal strain, γ, is the change in relative length, Δl, of a material compared to its original length, l. This relationship in changing length to determine strain is shown below:

$$\frac{\Delta l}{l} = \gamma \qquad [5]$$

From these relationships that describe stress and strain, [Equation 3] can be rewritten as:

$$\sigma = \frac{kl}{A}\gamma \qquad [6]$$

In [Equation 6], the term $\frac{kl}{A}$ is also known as the proportionality constant, and describes the linear relationship between stress and strain. This relationship is important for understanding the magnitude of deformation resulting from an applied load. The material property Modulus of Elasticity, E, describes how resistant a material is to out-of-plane deformation. It is affected by stress and strain and this relationship is shown below:

$$E = \frac{\sigma}{\gamma} \qquad [7]$$

The class of equations that describes the relationship of the stress and strain components within an orthotropic material is named "constitutive relations". Due to its orthotropy, wood experiences different properties in three material directions due to its three mutually perpendicular planes. Because of this, wood has three elastic moduli with different magnitudes based on material direction. The three elastic moduli are E_R, E_L, and E_T describing resistance to deformation caused by an applied load in the radial, longitudinal and tangential direction, respectively. Using Modulus of Elasticity (MOE) and other constitutive relationships normalizes the concepts of stress, strain, and deformation into quantifiable material properties.

The next material property related to wood's elastic behavior is the relationship between shear stress and shear strain. On the microscopic level, shear stress is the individual wood cells "slipping" past its adjacent cells (Shumulsky and Jones 2011), causing an angular shape change.

Bodig and Jayne define modulus of rigidity, G, "as a shear stress which causes a unit shear strain in the material" (1982). Its equation is given as the proportionality constant between shear stress and shear strain and is shown below:

$$G = \frac{\sigma_s}{\gamma_s} \qquad [8]$$

Like MOE, orthotropic wood also has three shear moduli: G_{LR}, G_{TR}, and G_{LT}. The subscripts represent shear stress and strain in the principal directions based on where the load is applied and then by which direction deformation occurs, respectively. For example, G_{LR} represents an application of a shear stress in the longitudinal direction and describes subsequent deformation along the radial direction. The modulus of rigidity describes a material's stiffness in shear, or its resistance to shear forces, in these directions.

To determine a material's Modulus of Elasticity and Rigidity, non-destructive experimental methods are utilized. The moduli are determined after collecting data from a testing machine. During the test, as a load (stress) is applied and measured, resultant deformation (strain) is simultaneously measured and graphed by the computer. An example of this stress-strain curve that would be seen with this type of experiment with is shown in Figure 2.2.4.

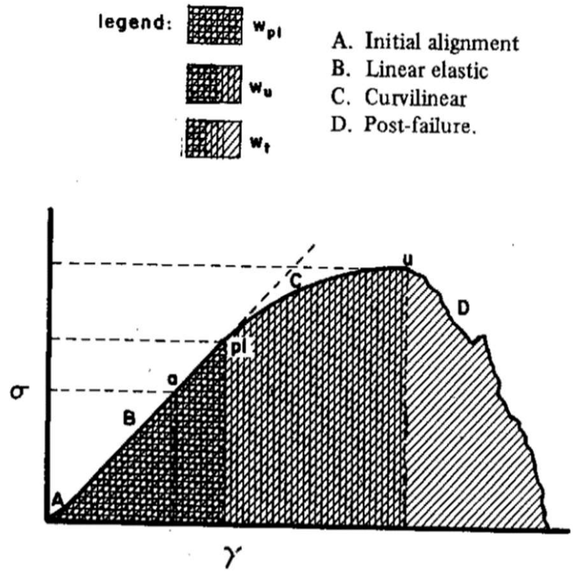

Figure 2.2.4: Characteristics of the stress-strain curve (Bodig and Jayne 1982).

As also seen in the load-deformation relationship of elastic-plastic materials (Figure 2.2.4A), Figure 2.2.4 exhibits the typical loading characteristics resulting from mechanical tests on wood. This graphical representation of wood's stress and strain values under load is divided into regions to describe the stages of testing.

After the load head aligns on the specimen (Region A, Figure 2.2.4), Region B shows stress and strain increasing at a proportional rate. This region demonstrates the linear elastic behavior of wood. Any loading that occurs in this region is completely recoverable. Moving along the curve, the point, *pl*, is the material's proportional limit. This point defines when the relationship between stress and strain is no longer linear. Beyond the proportional limit, strain begins increasing at a faster rate than stress, as seen in the curvilinear relationship of Region 3.

As the load continues to increase, ultimate failure is reached at point *u*. Past this point, Region D represents permanent deformation of the material which results from inducing increased stress and strain on already damaged wood cells.

From the stress-strain curve presented by Bodig and Jayne in Figure 2.2.4, mechanical properties of wood can be derived from the constitutive relationships it describes (1982). The modulus of elasticity, *E*, is determined by taking the slope of the line tangent to the linear Region B. Similar to [Equation 7], the relationship is given as:

$$E = tan\ \alpha = \frac{\sigma_{pl}}{\gamma_{pl}} \qquad [9]$$

When the machine is testing the material in shear, this same definition applies to shear stress and shear strain curves. In this case, the slope represents the modulus of rigidity, *G*, rather than of modulus of elasticity:

$$G = tan\ \alpha = \frac{\sigma_{pl}}{\gamma_{pl}} \qquad [10]$$

The last elastic material property to associate with other constitutive laws is Poisson's ratio. As describes by Bodig and Jayne, the phenomenon of lateral contraction of a rod as it elongates is a phenomenon known as Poisson's effect, discovered in 1760 by French scientist Denis Poisson. It is described by the ratio of passive to active deformation and is defined:

$$\nu_{ij} = \frac{\gamma_j}{\gamma_i} \qquad [11]$$

where ν_{ij} is Poisson's ratio for the passive strain, γ_j, in the *j*-direction where an active strain, γ_i, is caused by a uniaxial load in the i-direction (1982). Resultant deformation on the rod described by Poisson's effect is illustrated in Figure 2.2.5.

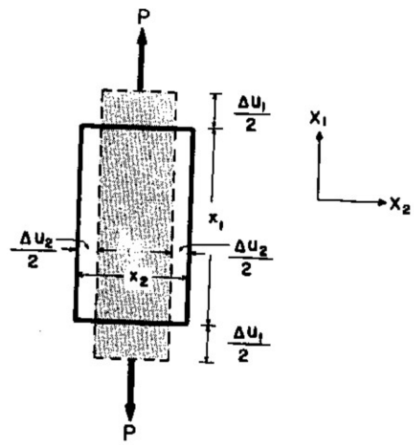

Figure 2.2.5: An applied uniaxial load results in Poisson's effect (Bodig and Jayne 1982).

In Figure 2.2.5, the application of tension load, *P*, causes elongation (Δu_1) in the active direction (x_1). With this, there is resultant contraction (Δu_2) in the passive direction – the direction where the load is not applied (x_2) – which occurs perpendicular to the loading axis. The diagram's resultant strains are $\gamma_1 = \frac{\Delta u_1}{x_1}$ and $\gamma_2 = \frac{\Delta u_2}{x_2}$. Using [Equation 11], the resultant Poisson's ratio in Figure 2.2.5 would be $\nu_{12} = \frac{\gamma_2}{\gamma_1}$.

Bodig and Jayne (1982) describe Hooke's Law for wood as a generalized mathematical statement used to relate each stress component to its strain component -- based on the assumption that stress and strain components are linearly related. This matrix formula uses the summation of the observations made from computing strains as linear functions of stresses.

The application of a normal stress, σ_1, produces 3 normal strains, γ_1, γ_2 and γ_3. The orthogonal strains are γ_2 and γ_3 and they are caused by the presence of internal stresses due to Poisson's effect.

As stated by Bodig and Jayne (1982), applying Hooke's Law in its simplified form to wood composites holds true if these four qualifiers are met:

1. Only small amounts of deformation is allowed

2. Uniform temperature must be maintained throughout entire composite

3. The composite is homogenous and has uniform density throughout

4. No coupling between stress components is allowed.

The parameters to constitute Hooke's Law are expressed in two forms: strains as a linear function of stress (compliance coefficients) or stress as linear functions of strains, known as the stiffness coefficient parameterization. In the latter, the six independent stresses are linearly related to six independent strains and expressed in the stiffness form of the law as a matrix equation:

$$\begin{bmatrix} \sigma_1 \\ \sigma_2 \\ \sigma_3 \\ \sigma_{23} \\ \sigma_{13} \\ \sigma_{12} \end{bmatrix} = \begin{bmatrix} C_{11} & C_{12} & C_{13} & C_{14} & C_{15} & C_{16} \\ C_{21} & C_{22} & C_{23} & C_{24} & C_{25} & C_{26} \\ C_{31} & C_{32} & C_{33} & C_{34} & C_{35} & C_{36} \\ C_{41} & C_{42} & C_{43} & C_{44} & C_{45} & C_{46} \\ C_{51} & C_{52} & C_{53} & C_{54} & C_{55} & C_{56} \\ C_{61} & C_{62} & C_{63} & C_{64} & C_{65} & C_{66} \end{bmatrix} \begin{bmatrix} \gamma_1 \\ \gamma_2 \\ \gamma_3 \\ \gamma_{23} \\ \gamma_{13} \\ \gamma_{12} \end{bmatrix} . \qquad [12]$$

The stiffness matrix form of Hooke's Law shows 21 independent parameters, so further simplification of this equation is necessary. Due to the symmetrical nature of the orthotropic wood composites, $S_{ij} = S_{ji}$, Hooke's law can be simplified, and nine parameters become sufficient enough to describe the three-dimensional elastic behavior of wood.

The most convenient way to express Hooke's law is in its matrix compliance form with strain as a linear function of stress, shown below:

$$\begin{bmatrix} \gamma_1 \\ \gamma_2 \\ \gamma_3 \\ \gamma_{23} \\ \gamma_{13} \\ \gamma_{12} \end{bmatrix} = \begin{bmatrix} S_{11} & S_{12} & S_{13} & 0 & 0 & 0 \\ S_{12} & S_{22} & S_{23} & 0 & 0 & 0 \\ S_{13} & S_{23} & S_{33} & 0 & 0 & 0 \\ 0 & 0 & 0 & S_{44} & 0 & 0 \\ 0 & 0 & 0 & 0 & S_{55} & 0 \\ 0 & 0 & 0 & 0 & 0 & S_{66} \end{bmatrix} \begin{bmatrix} \sigma_1 \\ \sigma_2 \\ \sigma_3 \\ \sigma_{23} \\ \sigma_{13} \\ \sigma_{12} \end{bmatrix}. \qquad [13]$$

This condensed form of the equation shows that several of the compliance parameters for orthotropic materials are zero. The generalized equation to represent the condensed form of this matrix is $\gamma = S\sigma$. For normal stresses, the coefficients S_{ij} represents the linearized slopes of stress-strain curves. With application of shear stresses, the compliance coefficients S_{44}, S_{55}, and S_{66} are the linearized slope of the shear stress-strain curve diagram.

An application of one shear stress in an orthotropic medium results in in one shear strain in the same direction of the applied stress. For example, the application of a stress σ_{12} only produces a shear strain γ_{12} and its magnitude is denoted $\gamma_{12} = S_{66}\sigma_{12}$.

Expanding on the compliance matrix [Equation 13], material directions replace numerical subscripts. In addition, material elastic parameters related to the compliance and stiffness coefficients are substituted. Hooke's Law for Wood takes this following form:

$$\begin{bmatrix} \gamma_L \\ \gamma_R \\ \gamma_T \\ \gamma_{RT} \\ \gamma_{LT} \\ \gamma_{LR} \end{bmatrix} = \begin{bmatrix} \frac{1}{E_L} & -\frac{\nu_{RL}}{E_R} & -\frac{\nu_{TL}}{E_T} & 0 & 0 & 0 \\ -\frac{\nu_{LR}}{E_L} & \frac{1}{E_R} & -\frac{\nu_{TR}}{E_T} & 0 & 0 & 0 \\ -\frac{\nu_{LT}}{E_L} & -\frac{\nu_{RT}}{E_R} & \frac{1}{E_T} & 0 & 0 & 0 \\ 0 & 0 & 0 & \frac{1}{G_{RT}} & 0 & 0 \\ 0 & 0 & 0 & 0 & \frac{1}{G_{LT}} & 0 \\ 0 & 0 & 0 & 0 & 0 & \frac{1}{G_{LR}} \end{bmatrix} \begin{bmatrix} \sigma_L \\ \sigma_R \\ \sigma_T \\ \sigma_{RT} \\ \sigma_{LT} \\ \sigma_{LR} \end{bmatrix} \qquad [14]$$

Modulus of elasticity is represented in the three material directions by E_L, E_R, and E_T. Poisson's ratio is represented by v_{ij} with transverse strain in the j-direction when stressed in the i-direction. The six ratios used to describe the Poisson effect in wood are: υ_{RL}, $\upsilon_{TL}, \upsilon_{LR}, \upsilon_{TR}, \upsilon_{LT}$, and υ_{RT}. However, due to the symmetric relationship of the compliance matrix ($S_{ij} = S_{ji}$), only three of the six ratios are independent. The modulus of rigidity, G, is used to describe the three shear directions (G_{RT}, G_{LT}, and G_{LR}) resistance to deformation in shear.

The elastic properties of wood composites based on wood's constitutive properties are discussed in textbooks (Bodig and Jayne 1982), (Suchsland 2004), (USDA 2010) and is published in research studies (Janowiak, Hindman, and Manbeck 2000).

Elastic parameters used describe an anisotropic asymmetric laminate are discussed by Bodig and Jayne. They begin this analysis by defining a simple, three-layer, symmetric, orthotropic composite. Assumptions are made to simplify the analysis of rectangular laminates. The analysis of laminates is based on the elastic characteristics of each individual laminae, that is assumed to be homogeneous and of uniform characteristics (1982).

The second assumption made by Bodig and Jayne for the analysis of laminate's elastic properties is related to the adhesive bonding system. The bond-line between individual laminae is assumed to be perfectly rigid, and despite inconsistencies in the manufacturing process, is always to be assumed uniform. The adhesive's effect on the elastic properties of the laminate system is always assumed to be negligent (1982).

Further research and analysis on the effect of elastic properties based on wood mechanics and constitutive laws in wood composites is the next area to explore to investigate this warpage phenomenon. Future research will help to better understand the relationships of how these factors and characteristics effect the performance of wood-based composites.

2.3 Review of Composite Materials

There are several textbooks that discuss the fabrication and mechanics of composite materials (Jones 1975), (Bodig and Jayne 1982), (Sellers 1985), (Suchsland 2004), (Shmulsky and Jones 2011). The benefits of producing wood composite products from solid wood is also discussed. In this experimental research study, the warpage behavior of wood composites is influenced by a variety of characteristics, including the panel's make-up and fabrication processes, all to be discussed in this section.

As described in his textbook, Jones states there are three types of composites that are categorized by material composition and fabrication process that produce a final product. The three types of composites are defined as the following: fibrous composites (fibers embedded in a matrix); particulate composites (particles embedded in a matrix); and finally, laminated composites, which consists of layers of various materials used to combine the best attributes of each layer of material to obtain a more useful product (1975).

When considering the composite classification for engineered wood products, fiberboard and particleboard are examples of the fibrous and particulate composite class, respectively. Other engineered wood-panel products, such as plywood or Laminated Veneer Lumber (LVL), are an example of a laminated composite, and veneer-based wood products are the composite under analysis in this study.

The manufacture of veneer for laminated composites is described by Shmulsky and Jones. The production of veneer for structural composites is notably peeled on lathes, although sliced veneer is the older method for production, and still used for visual-grade veneer. Rotary lathes are used to provide a continuous peel of the tree's circumference by angling a knife and applying a pressure bar to obtain the desired veneer thickness. Veneer for structural wood panels is commonly peeled to thicknesses ranging from 1/10 to 1/6” (2011). The veneer peeling process is outlined while the orthotropy directions are presented respect to the rotary lathe in Figure 2.3.1.

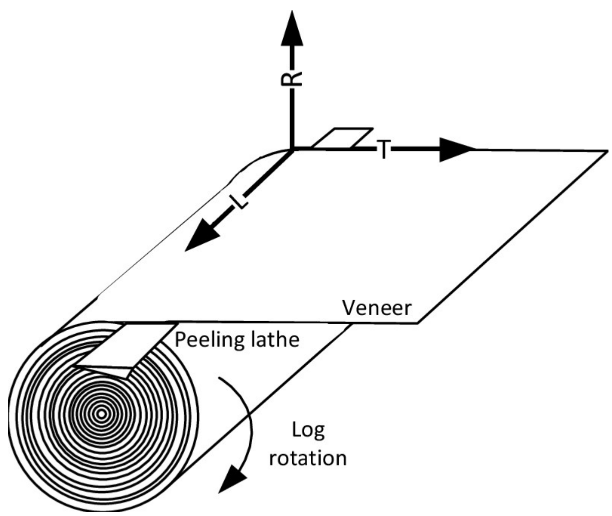

Figure 2.3.1: Rotary peeled veneer procedure (Tomppo 2013).

The earliest wood-laminated product was veneered lumber – a two-ply product fabricated by adhering a sheet of sliced veneer to a piece of lumber designed to improve the performance of solid wood (Suchsland 2004). The grain orientation in both pieces is the same and this type of fabricated wood product is still used today in the manufacture of doors or cabinetry.

One product that utilizes this concept in a modernized way is the engineered solid-core door. This product utilizes a cheaper, less attractive engineered wood product, such as particle board, to provide uniformity and strength to the door’s core. Thin, wood veneers are then adhered to all four sides to provide additional stability to the door, but more importantly for the product’s marketability, the door’s aesthetics are also improved significantly.

Throughout the years, additional engineered wood products have been developed to meet greater structural and architectural demands. For example, in order to meet extended lengths required for floor joists in modern light-frame residential construction, engineered I-Joists were developed. By combining two engineered wood products, the final product proved to have higher strength capacity than solid wood in the same loading environment. By utilizing OSB and LVL for its major components instead of solid wood, the end-product is lightweight, resulting in lower shipping costs (Shmulsky and Jones 2010).

In his textbook on composite mechanics, Jones describes materials that are considered "composite" when two or more materials are combined to form a material that is more useful (1975). With a general understanding of how composites are fabricated, now it is important to highlight their benefits. Jones states that the greatest advantage of composite materials has on their constituents is that by engineering a composite, the best qualities are preserved, often resulting in qualities that neither constituent material possesses (1975). One example is the increased dimensional stability capacity of composites compared to untreated solid wood.

Due to their increased, randomized grain orientation, engineered wood products with cross-laminations are more isotropic than solid wood or unidirectional fiber products, like LVL (Shmulsky and Jones 2011). Cross-ply lamination alters the warpage behavior from that seen in solid wood (Suchsland 2004), improving the dimensional stability of the product.

In their textbook on wood and wood composite mechanics, Bodig and Jayne address the potential importance of modeling wood composites (1982). The purpose of the modeling is to identify the major factors that alter composite's behavior. In addition, the properties of certain characteristics can be simplified from models (Bodig and Jayne 1982).

Bodig and Jayne describe the first theoretical modeling for wood composites as mathematical methods for predicting plywood's mechanical properties (1982). The predictions of the composite materials were made possible by using the individual veneer properties available at the time. The authors report that the modeling process is often limited to a system of only basic elements (1982), which has been expanded on throughout the years, and is even the topic of this research study.

2.4 Studies on Wood Panel Deformation and Warpage

The warpage of wood panels is an industry-wide issue that has been present since the development of wood-based panel products. Due to irreversible out-of-plane deformation that results when wood panels are exposed to changes in moisture content or environmental conditions, the flatness required for panel products becomes compromised.

The shrinking and swelling behavior of laminated wood products is discussed in textbooks (Bodig and Jayne 1982), (Suchsland 2004), (USDA 2010). In unidirectional engineered wood products, such as laminate doors, unless the wood substrate and veneer have drastically different properties, this type of lamination does not affect warpage behavior (Suchsland 2004).

Many researchers have worked to begin to understand this warpage phenomenon. In one early endeavor, Cave (1972) developed a theory to determine the relationship between shrinkage in transversely isotropic composites and variation in moisture content. The effect of variable, microscopic wood properties have on determining a predictable shrinkage model is also discussed. He notes that microfibril angle, S_2 wall layer thickness, cellulose concentration, and the stiffness of the intercellular matrix all affect wood shrinkage.

Following previous studies of determining warpage behavior in wood, it has become more common to use previous findings to develop predictive warpage models, and later, validate the estimated deformation experimentally (Lang 1993; Lang, Loferski, and Dolan 1995; Cai and Dickens 2004).

In 1993, models are developed to quantitatively measure the global deflection of wood-based composite sheathing, specifically for OSB and plywood, that are exposed to changes in relative humidity (Lang 1993). The models are experimentally validated through three-dimensional surface scanning before and after moisture exposure using LDVT technology. In total, 765 nodal points are marked across the testing plane to measure and record deflection measurements consistently for model validation throughout experimentation.

An experiment (Lang, Loferski, and Dolan 1995) is conducted in response to out-of-plane deformation noticed in wood-based composites floor systems exposed to an imbalance in humidity level at their opposite faces. The theoretical, mechanics-based procedure is developed to predict a panel's resultant free hygroscopic warpage. Following the theoretical predictions, experimental validations on a 5-ply OSB panel exposed to 95% humidity on only one side coincide with the estimated deformation. A measurement scheme for the cylindrical deformations of the panel is also developed to measure against the theoretical predictions.

The experimental procedure is designed to validate the theoretical radius of curvature prediction method for the case of a panel with non-symmetric moisture exposure. Only one side of the panel is exposed to 95% RH and a nonsymmetric moisture gradient through the panels' thickness is ensured by inserting a polyethylene vapor barrier and taping down the rest of the panel.

To verify the theoretical predictions, the experimental procedure consists of measuring the moisture content of the exposed test panels at three depths with an electric conductance moisture meter over several locations on the panel's surface. The moisture content measured developed regression equations that estimate the gradient in moisture content throughout the panel's thickness before and after RH exposure.

Prior to and following the treatment period, a measure of the panel's surface was conducted. The deformation measurements, identical to Lang (1993), were made from placing the panel on a fixed, aluminum bar laboratory test frame. A LVDT measured the out-of-plane deflection at 765 points on the panel's surface, utilizing a linear rotary potentiometer to locate position. The measurement of interest, radii of curvature, was determined for both X-Y directions using the collected deformation data. From this, curvature predictions for plywood and OSB were confirmed for both directions. Plywood's curvature prediction, however, proved to be less accurate than OSB with the authors attributing this to the increased variability of veneers compared to randomized placement of wood flakes (Lang, Loferski, and Dolan 1995).

This study of experimentally validating theoretical moisture gradient prediction methods for warpage of wood composites follows a similar approach to this project. The out-of-plane deformation measurements are compared to the modeling predictions using the theoretically determined equations. The moisture gradients of interest, however, are not congruent with this project's model that utilizes a through-thickness moisture gradient that is symmetric.

A two-dimensional warping model based on wood composite mechanics and the simulation of various engineering parameters is developed (Cai and Dickens 2004). The model is based on prior one-dimensional mathematical models that were used to investigate warping problems. However, by only measuring one-dimensional deformation, lateral strain and the effect of Poisson's ratio is ignored which is incorrect to use for three-dimensional orthogonal panels. The developed model is used to predict the effect different material properties have on warping wood.

The prediction and determination of moisture gradients and their effect on the warpage of wood panels has also been studied (Cai and Dickens 2004; Jakieła, Bratasz, and Kozłowski

2007). In their study to model the warpage of composites, Cai and Dickens note the effect increasing moisture gradient has on wood deformation. Presented in Figure 2.4.1, they use a computer-simulated warpage model to output the relationship between increasing moisture gradient concentration and resultant, center deflection in inches.

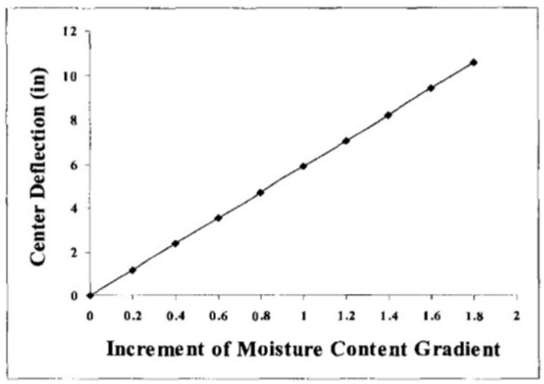

Figure 2.4.1: Relationship of increasing moisture content gradient's effect on center deflection (Cai and Dickens 2004).

The relationship in Figure 2.4.1 shows that if the concentration of the through-thickness moisture gradient is greater, more deformation will occur. The relationship between an increasing moisture gradient and resultant warpage is linear (Cai and Dickens 2004).

Investigating further into experiments concerned with changes in wood's surrounding environmental conditions, one study models moisture movement in wood based on variations in relative humidity (Jakieła, Bratasz, and Kozłowski 2007). Previous models at the time ignored the stresses caused by internal structural restraint, which is an effect of material anisotropy in moisture-induced dimensional changes. The material properties needed to model moisture differentials in wood are the equilibrium moisture content (EMC) and moisture diffusion coefficients.

2.4.1 Review of Theoretical Warpage Prediction Model

Most recently, Phase I of this Geometry and Mechanics of Panel Warpage project has been completed (Wood 2019) and published (Wood and Hanna 2020). From an engineering mechanics and soft matter physics perspective, their study on the swelling gradients of anisotropic thin plates and shells was inspired by engineered wood products exposed to moisture. By investigating the warped shapes of anisotropic plates with variation in moisture gradient patterns, an elasticity model is created to theoretically predict the warped shapes for anisotropic materials with varying moisture gradients.

The current study characterizes the warped shapes associated with moisture content changes during the manufacture of engineered wood products, specifically the geometries of the warped specimens. The equilibrium shape for the deformation induced by a given swelling function is found to be either twisted or axisymmetric. Using geometrical characterizations, a qualitative argument is provided for producing the warpage behaviors.

An axisymmetric configuration means to be symmetric about one axis, causing a cylinder-like shape. Shown in Figure 2.4.2, plastic models with slits simulating grain direction of anisotropic plates were used to simulate middle shrinkage and expansion scenarios.

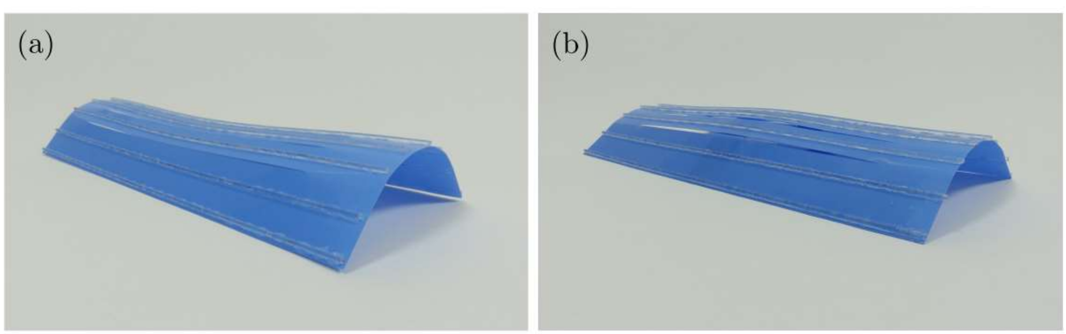

Figure 2.4.2: Plastic plate models simulating middle shrinkage (a) and middle expansion (b) (Wood 2019).

In Figure 2.4.2(a), middle shrinkage is produced by adhering the sliced splits together with tape in the plate's center. For the middle shrinkage scenario, swelling is greatest toward the end of the plate resulting in an overall saddle-like, axisymmetric shape. Additionally, Figure 2.4.2(b) demonstrates the middle swelling case by moving the slits about the plates center apart from one another, and this concentrated middle expansion causes a spherical dome-like shape with plate edges approximating cylinders. Both cases are considered to have axisymmetric geometries because the plates' shapes are symmetrical about the center axis.

With qualitative analysis of the unidirectional plates in mind, the theoretical warpage prediction model is generated in a multiple step process (Wood and Hanna 2020). The step of relevancy to this project is the methodology involved in defining the model's system. The model's system definitions are used to design the warpage experiment conditions.

The theoretical plate under analysis in the model is designed to simulate anisotropic LVL panels made up of stacked, unidirectional sheets of veneer. The plate schematic (seen in Figure 3.2.1) was modeled with dimensions length = $2L$ and width = L (for an aspect ratio of 1:2) with a thickness of $h << L$. Material coordinate x describes the fiber direction and y is the planar transverse direction, or the direction perpendicular to the fiber orientation. Swelling occurs in the y-direction and the swelling gradients of interest vary along the x-direction with the requirement that x is an arc length coordinate.

With swelling gradients varying only on the x coordinate, a programmable swelling metric is defined that eliminates all stretching energies:

$$dx^2 + U(x)^2 dy^2$$

The $U(x)^2$ term is an interchangeable swelling function – selected by determining $U(x)$ – that describes that panel's surface and changes based on the x-coordinate under analysis.

Different functions are substituted to state whether a shrinking or swelling case -- relative to the outside of the panel -- is under analysis.

To investigate middle shrinking and swelling cases, the following *U(x)* expression is used.

$$U(x) = 1 + a \operatorname{sech}(cx) \qquad [15]$$

Controllable parameters are introduced in interchangeable *U(x)* functions. In Equation 15, parameter *a* defines the magnitude and direction of swelling. The direction of the swelling behavior is determined by the sign of the magnitude parameter. A positive *a* results in middle expansion, which swells the plate, and a negative *a* results in middle contraction, or shrinkage of the plate. Parameter *c* controls the gradient of the swelling. By increasing or decreasing *c*, the amount of area that shrinks or swells is decreased or increased, respectively.

Using the same swelling function, $U(x) = 1 + a \operatorname{sech}(cx)$ where $\chi = 0$, parameter values *a* and *c* are selected. An example described by Wood (2019), a function is used to simulate the warpage of yellow-poplar LVL panels. Material properties selected for incorporation into the embedded energy expression include Modulus of Elasticity, shear moduli, and Poisson ratios. The reduced stiffness calculations [Equations 16-19], determined by Wood, incorporate material property values such as Modulus of Elasticity and passion ratios, and are plugged into the final energy expression.

$$C_{(11)} = \frac{E_x}{(1-\upsilon_{xy}\upsilon_{yx})} \quad [16] \qquad\qquad C_{(22)} = \frac{E_y}{(1-\upsilon_{xy}\upsilon_{yx})} \quad [17]$$

$$C_{(12)} = \frac{(\upsilon_{xy})(E_y)}{(1-\upsilon_{xy}\upsilon_{yx})} \quad [18] \qquad\qquad C_{(66)} = G_{xy} \quad [19]$$

To simulate the warpage, the bending energy expression for this case is numerically minimized with respect to η and χ. Using the results from the reduced stiffness calculations, the dimensionless form of the energy is described as:

$$\frac{24E}{h^3 C_{(11)}} = \iint \sqrt{g}\, dx dy \left[(b^x_x)^2 + 4\frac{C_{(66)}}{C_{(11)}} b^x_y b^y_x + 2\frac{C_{(12)}}{C_{(11)}} b^x_x b^y_y + \frac{C_{(22)}}{C_{(11)}} (b^y_y)^2 \right] \qquad [20]$$

In this example, in addition to including the material properties through the incorporating reduced stiffness calculations, the parameter values of $a = \pm\, 0.05$ and $c = 4$ are selected for the *U(x)* swelling function. The resultant shapes are axisymmetric ($\chi = 0$), with term χ describing the twisting behavior as zero, or none. Below are resultant numerical surface plots that show the gradient $c = 4$ with Figure 2.4.6a representing $a = -0.05$, a middle shrinking scenario, and Figure 2.4.6b as $a = 0.05$, a middle swelling scenario.

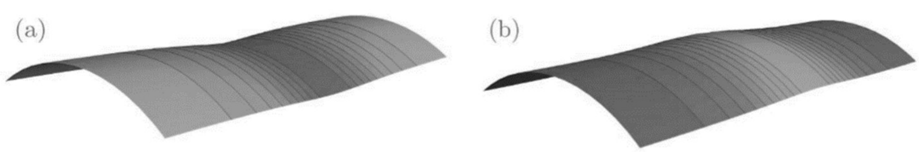

Figure 2.4.3: Surface plots resulting from integration of the function *U(x) = 1 + a sech (cx)* over the energy expression in [Eq. 20] (Wood 2019).

In the surface plots, the moisture content gradient is represented by lighter colored regions to show swelling and darker colored regions to show where the panel shrinks. Because the swelling gradient, *c*, is the same in this example, the magnitude of swelling is consistent. However, in the case where *a* is negative, there is shrinking in the center of the panel and swelling toward the outer regions whereas the positive *a* case results in middle expansion.

Utilizing programmable swelling functions allows for the analysis of in-plane swelling gradients on anisotropic plates. By modeling elastic plates exposed to hypothetical shrinking or swelling patterns, the resultant warped geometries are determined. Predictions as to how a panel will react when exposed to moisture can be determined using this incompatible elasticity model. From the conclusions stated in previous works (Wood 2019) and (Wood and Hanna 2020), experimental design for warpage experiments inspired by the theoretical models is discussed in the subsequent chapters.

2.5 Deformation Monitoring Techniques using 3D Scanning

Several methods for measuring the out-of-plane deformation of wood panels caused by changes in moisture content are investigated for use in this project. The techniques explored include laser/optical interferometry, digital image correlation and LVDT (Linear Variable Differential Transformer) technology, and three-dimensional scanning technology is selected.

Three-dimensional scanning technology is one way to monitor and track the deformation of objects. The usefulness and relevancy of 3D scanning for the manufacturing industry and reverse engineering processes is discussed in papers (Guo-hui 2008), and (Gerbino, et al. 2015).

The principles behind 3D scanning technology are discussed by Georgopoulos and his colleagues (2010). To collect surface deformation data, the scanner emits a pattern of light onto the object's surface using either an LCD projector in structured light scanning or a sweeping laser in laser scanning. Inside of the scanner, cameras offset from the projector capture the shape of pattern of light's deformed shape and the distances of the surface points in the field of view are recorded at an angle α (Figure 2.5.1).

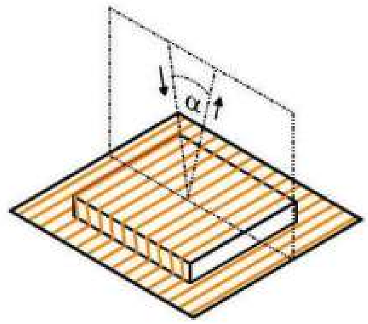

Figure 2.5.1: Three-dimensional scanning triangulation principle (Georgopoulos, et al. 2010).

The triangulation principle, illustrated in Figure 2.5.1, is the technique used to calculate the distance of the angles at every point on the line of the scanner's projected pattern. Once the reflected light is collected by the camera, a complex algorithm calculates the distance at each point in the pattern and a computer reconstructs the data to create a visualization of the collected deformation data, also known as a mesh (Georgopoulos, et al. 2010).

The purpose for 3D laser scanning is discussed by Gerbino and his colleagues. Optical scanning devices are used to digitally reconstruct three-dimensional, real world objects. Objects of complex shapes and sizes, such as large statues or buildings, can also be reconstructed using high-end scanning technologies. Three-dimensional laser scanning is a non-contact method for acquiring the points of an entire object (Gerbino, et al. 2015).

Guo-hui describes the basic functions involved in the 3D laser scanning process. Laser is emitted from the scanner and then reflected by the rotation axis' orthogonal mirrors onto the object. This 3D laser scanning technology was utilized in an experiment (Guo-hui 2008) to monitor deformation. The benefit of utilizing this method is shown through the following experiment. By using a scanner, the coordinates of an objects surface points are measured.

During the process, multiple surface points can be collected at once – up to 1,000 points per second. Data is collected in substantially less time compared the original, hand-done methods such as drafting and architectural drawing. After measurements are recorded, the system displays them in a point cloud format which makes digitally modeling the object possible (Guo-hui 2008).

In their paper, Gerbino and his colleagues describe 3D laser scanning process from the perspective of the post-scan 3D inspection process. The manufacturing industry is increasingly relying on this technology to be able to monitor the quality of any given product or process (Gerbino, et al. 2015).

As discussed by Gerbino and his colleagues, there are internal and external factors that affect the quality of 3D scanning data. Internal factors relate to elements internal to the scanning device such as the resolution and accuracy of the scanner (Gerbino et al. 2015). These values are obtained from the individual scanner's manufacturer because they differ based on the quality and price point of the device.

The external factors that affect scanning quality include properly selecting appropriate scanning parameters, sufficient ambient lighting, surface characteristics of the object being scanned, and the relative position of the sensor to the surface. These factors all influence the ability to extrapolate the surface geometry data reconstructed from the mesh (Gerbino, et al. 2015).

The EinScan-Pro is a multi-functional handheld 3D scanner. The basic operating principals and procedures are described in the user manual (SHINING 3D N.d.). As setup begins, there are many options to select through based on the object under analysis. For example, there are four scanning modes meant for various objects and situations. Each mode has its own associated accuracy and point distance. Accuracy describes how close the scanner gets to correctly recording the surface points compared to its actual location. Point distance defines how close together or far apart the scanner can scan and record surface measurements.

The four scanning modes are described as the following:

1) Handheld High-Definition (HD) scan - for objects with rich details and that are difficult to move; captures at high accuracy and resolution. Its accuracy is 0.1 mm with a point distance between 0.2 mm and 3.0 mm
2) Handheld rapid scan – the quickest scanning mode; less accurate than other modes. This mode's accuracy is 0.3 mm and the point distance varies between 0.5 mm to 3.0 mm
3) Fixed scan (with turntable) – this method conducts a 360^{o} automatic scan "within seconds." It is meant for small objects, within size of 200 mm^3, that can fit on a rotating turntable. The fixed single scans accuracies are more precise than the handheld methods at 0.05 mm. The point distance is 0.16 mm.
4) Fixed scan (without turntable) – scanner is on a stand; provides for least amount of human error. This scan method is meant for objects larger than the turntable, or over the size of 200 mm^3. The fixed scan method with and without the turntable has the same accuracy magnitude and point distance.

After a scan mode is selected, there are three types of align modes that determine how the scanner collects information during the scan. The first method is "feature alignment" and is suitable for objects with rich features on its surface. This scanning method is best used for large, unmovable objects like sculptures.

The second scanning method is "marker alignment". This method is intended for objects with plane and symmetric features. This scanning method relies on randomly dispersed reflective mark points to align the scanner for collecting surface geometry data. Placing at least four points per scan area, the marking points have a single scan range of 300 mm x 170 mm.

"Mixed alignment" is the last alignment type for the EinScan-Pro 3D scanner. This method is only used in the handheld rapid scan mode as this method works by the software switching between feature and marker alignment automatically based on object's surface.

Once a scan mode and alignment method is selected, the operation procedure for the scanner is quite simple with systematic prompts to guide one through set up and data collection. To begin in the scanning software, once connected to the computer, the EinScan-Pro device is selected, and next, the scan mode that is used for scanning analysis is selected. The desired resolution and align mode is given based on the object being scanned. Once selections are made, the process begins by previewing the scan and adjusting brightness and distance as necessary. Next, the scan will start, editing scan data along the way, and continue scanning until the entire surface geometry has been recorded.

To finish the scan, the point cloud data is exported as a .ASC file. This gives a script version of all the point data collected. With this data, the scanning program exports and saves a 3D mesh of the coordinates from the point cloud. Once the mesh is generated, the file is saved as the final scan. The mesh data can then be exported to a variety of file types that model the image as a composition of triangles and polygons.

After a scan is made using the EinScan scanning interface, the mesh data is exported into a file type that renders the model into a geometrical shape made of polygons (e.g., .OBJ, .STL, and. PLY) available for analysis with 3D inspection software. The procedure of determining the appropriate inspection software is outlined in chapter 4's methods.

Techniques to analyze 3D models rendered from meshes are investigated (Farin 2003). The analysis of surface curvatures and geometries using Computer Aided Geometric Design has progressed since its initial inception in the late 1950's. As new tools were produced to allow for machining of 3-dimensional shapes from solid blocks of wood and steel, the need to produce a computer-compatible visualization of the desired geometry was introduced (2003).

Theories regarding differential geometry and parametric surfaces had not yet been transcribed for their representation in Computer Aided Design. Early explorations into the use of curves and parametric surfaces initiated the field of Computer Aided Geometric Design, or CAGD. Utilizing concepts from differential geometry, the de Casteljau Algorithm is fundamental in designing surfaces and curvatures. Based on a relationship between algebra and geometry, this algorithm is the basis of CAGD, or the intuitive geometric reconstruction of objects (Farin 2003).

When utilizing computer implementation of designing surfaces and curvatures, the concept of a coordinate-free method is used. A coordinate system for an object defined by CAGD is based on the object of interest, not an arbitrary coordinate-system allowing for a more analytical approach when representing an object with computer-aided design programs (Farin 2003).

Presently, Computer Aided Geometric Design is now a much more streamlined process. With today's new software programs that are designed with object reconstruction principles in mind, CAGD is more powerful than ever before. The computer programs used to reconstruct scanned surfaces of wood consist of CAD-based software used for object reconstruction or reverse engineering purposes. The programs selected to analyze the surface geometries of the warpage experiment veneer specimens are listed in Figure 4.2.5.

2.6 Understanding the Problem

The ability to use engineered wood products in place of solid lumber provides many benefits, however, the development of new wood-based panels presents unique challenges. Engineering a new wood product is time consuming and expensive as extensive testing of many samples is required before mass-market production.

During the manufacturing process, panels are fabricated by assembling different materials each with their own unique, independent behaviors into one cohesive unit. Throughout the fabrication stage, the conditions of the manufacturing facility are be closely monitored and controlled. After the products leave the manufacturing environment's consistent conditions, problems concerning the panel's dimensional stability arise. A material is considered dimensionally stable if no warpage occurs following the manufacturing process due to changes in surrounding environmental conditions (Rindler, et al 2018).

In addition to processes used in production, it is important to understand the unique mechanical properties of wood composites. Factors that influence innate properties include wood species, wood quality based on cultivation and harvesting practices, the adhesive system used to bind the composite, type of wood element composing the composite (fibers, veneer, flakes, etc.), and the density of the final composite product (USDA 2010). The effects of the mechanical properties of wood composites on resultant warpage behavior is discussed thoroughly in the subsequent chapter.

Besides the wood material itself, other factors that are considered when observing warpage behavior include the adhesive system used, and additionally, the interactions of the properties between the individual components of a multi-layered composite product. On the microscopic level, hygrothermal loads occur when changes in moisture content causes stresses and deformation as water leaves or enters the individual wood cells (Lang 1981). Moisture differentials within wood panels cause internal stresses which induce dimensional changes and warpage. If observed panel deformation is too great, moisture-related defects compromise the final product and potentially, the reputation of the manufacturer (Cai 2003).

On a macroscopic level, wood-based composite products exhibit hygrothermal characteristics during changes in surrounding environmental conditions. This innate behavior observed in biological materials causes the wood panels to deform, unable to conform back into its original, flat shape. If hygrothermal behaviors occur during the manufacturing process and dimensionally stability exceeds the allowable tolerance for deformation, then the panel will not be able to be used for its designed application. Changes in surrounding environmental conditions causing dimensional-instability results in a waste in resources and revenue for the manufacturer.

Additionally, another common wood-based composite warpage occurrence results from in-plane contraction or expansion of the individual layers. When combining inhomogeneous materials into one cohesive panel, condition changes generate unbalanced stress and strain states between the different layers – beginning from the outer-most plies to the inner sections of the panel. Unbalanced conditions within a panel are instigated several ways such as changes in the surrounding environment, like temperature or humidity, sensitivity to moisture, or by certain chemicals that may have been used during the manufacturing process that may modify the material's ability to absorb or desorb moisture (Rindler, et al 2018). During the manufacturing process, it is important to maintain consistent conditions for each individual component prior to fabrication.

As manufacturing efforts for engineered wood products have scaled-up over the past century, so has the need for maintaining a consistent, dimensionally stable, and high-quality final product. However, controlling the quality of a naturally produced biomaterial is difficult. By understanding how wood composites are constructed and fabricated, insight is gained into how they might behave when exposed to changes in environmental conditions. With previous knowledge of wood warpage behaviors, experiments inducing and quantifying warped panel geometries are designed to investigate the resultant deformation caused by manipulations in the moisture gradient.

3.0 Development of Moisture Induction Methods

The first objective is to create and quantify moisture induction methods. Several subobjectives are completed to achieve the objective. Moisture induction methods are developed using parameters from the design of the warpage prediction model described by Wood (Wood and Hanna 2020). Methods are developed to measure moisture gradient concentration, and two different gradients are developed. The moisture gradient scenarios are statistically compared to each other to determine significance between the developed gradients. The developed gradients are used in Chapter 4 warpage experiments to test the effect of manipulation in moisture gradients on warpage.

The flow chart in Figure 3.1.1 outlines the procedures and methods required to achieve the first objective. Three subobjectives are used. The first subobjective is to develop moisture induction methods to produce controlled warpage as predicted by the model (Wood and Hanna 2020) (Wood 2019). Five species are selected, and four wetting methods are investigated to produce moisture-induced warpage.

The second subobjective is to evaluate the moisture induction methods to quantify each method’s effect on moisture content change. Each wetting method is tested on each species and two moisture content measurement methods are used to evaluate the moisture content change produced by the wetting methods. The difference in initial and final moisture content is used to quantify each method.

Using results from quantifying the moisture induction methods, the third subobjective is to create moisture gradients. A combination of wetting methods is strategically placed on the top and bottom surfaces of veneer to produce two gradients of varying magnitude: one high and one low concentration. The moisture gradients are used in Chapter 4 to induce warpage.

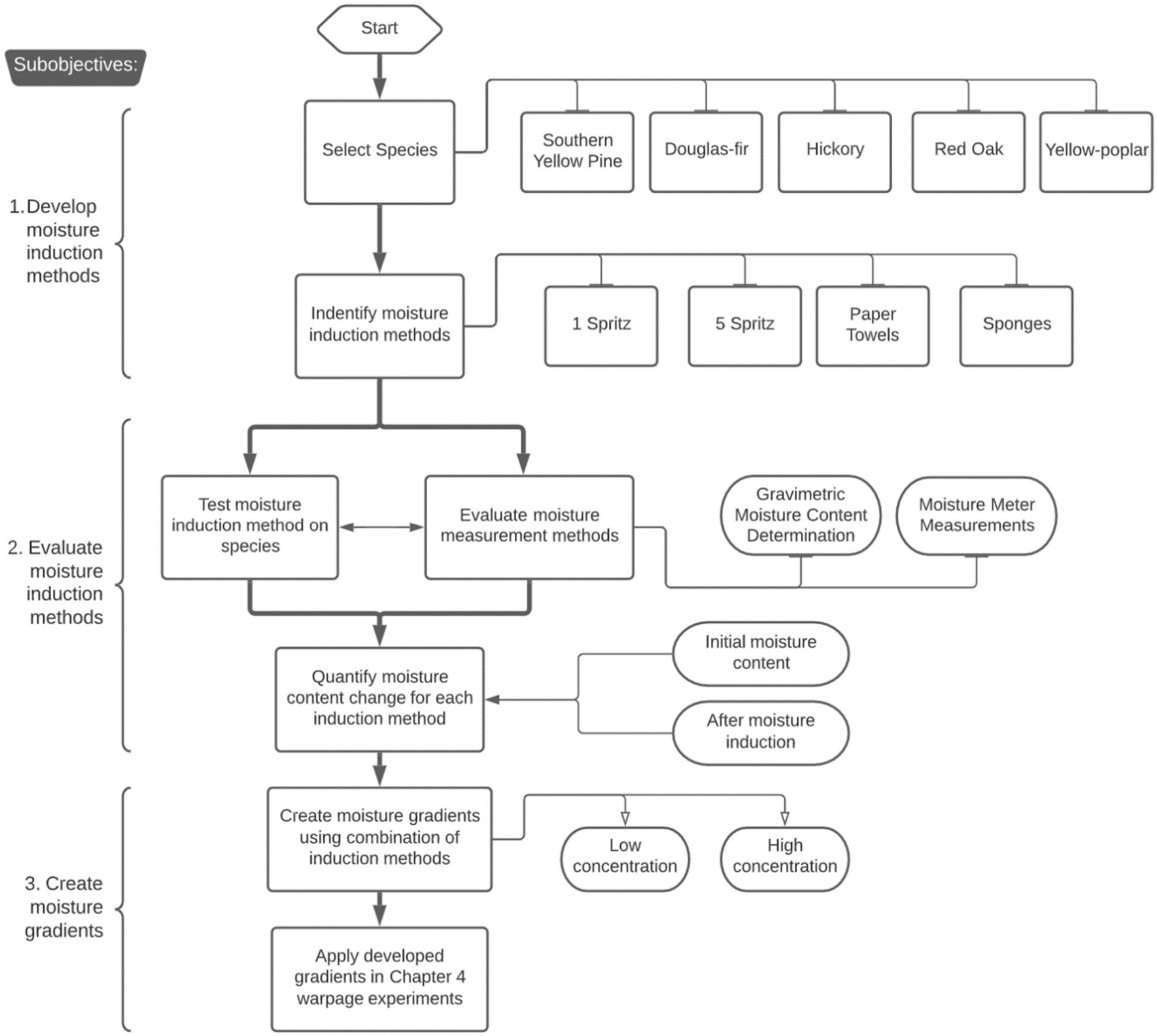

Figure 3.1.1: Flow chart outlining procedure for the Objective 1 by subobjective.

3.1 Materials

The list of veneer species and thicknesses used in the warpage experiments is shown in Table 3.1.1.

Veneer Species	Thickness
Hickory (*Carya spp.*)	0.0625”
Red Oak (*Quercus spp.*)	0.0625”
Yellow-Poplar (*Liriodendron tulipifera*)	0.0833”
Southern Yellow Pine (*Pinus spp.*)	0.167”
Douglas-fir (*Pseudotsuga menziesii*)	0.10”, 0.125”, 0.14”

Table 3.1.1: List of veneer materials to utilize during warpage experiments.

Five different veneer species are used during warpage experiments. The hardwood veneers -- hickory, red oak, and yellow-poplar -- were obtained from previous projects from Virginia Tech’s department of Sustainable Biomaterials. These species were selected due to their readily availability. Also, yellow-poplar is used in LVL manufacturing. The thicknesses available in hickory and red oak are limited because they are appearance grade veneers, not meant for structural applications.

Additionally, softwood veneers were obtained. Softwoods are commonly used to produce veneer-based panel products, so it was important to conduct warpage experiments on softwood species. To acquire the commercially relevant veneer species, Wood Based Composite Center industry partners were contacted. The southern yellow pine veneer is from Louisiana Pacific’s LVL mill in Wilmington, North Carolina obtained following a tour of their facilities. The Douglas-fir veneer in three thicknesses (1/8”, 1/10”, and 0.14”) was shipped to Blacksburg from Boise Cascade in Medford, Oregon.

The five different species of veneer in assorted dimensions are stored together before they are used. Because the materials were obtained from different sources, it is important for the veneers to remain together to standardize the storage conditions and equilibrate to the same moisture content. The panels were kept at room temperature (68-72°F) throughout the duration of the project, or two years. As seen in Figure 3.1.2, the sheets of veneer are stacked on a pallet to encourage flatness. Veneers were kept as flat as possible during storage because the initial geometry of the veneer is the initial flatness of the panel.

Figure 3.1.2: Veneer specimens' storage environment.

To investigate the effect of wetting methods on moisture content of the veneers, a Delmhorst J-2000 moisture meter and supplemental electrode are used. The Delmhorst 15-E is an 8-pin electrode with a 1/8" penetration depth – advertised as ideal for thin veneers. The meter has a moisture range of 6-40%. The meter and electrode used to measure moisture content are shown in Figure 3.1.2. In the photo on the right, a reading is taken with the attachment and moisture content is displayed on the meter.

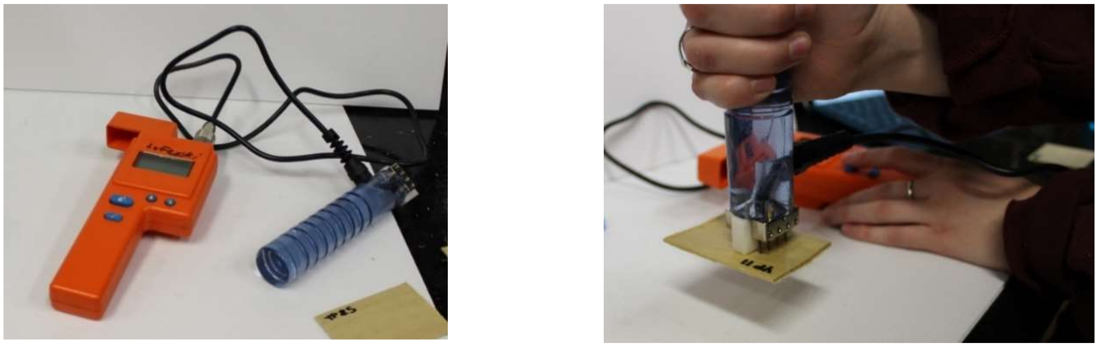

Figure 3.1.3: The Delmhorst J-2000 moisture meter and the 15-E attachment electrode.

3.2 Methods

The methods used to complete the first objective are described in this section. The first objective is to develop and quantify moisture induction methods to produce experimental warpage. The three subobjectives, outlined by the flowchart in Figure 1.1.1, required to complete the project's first objective are:

1) Develop moisture induction methods
2) Evaluate moisture induction methods
3) Create moisture gradients

Each subobjective is discussed in its own subsection for the methods and procedures required for completion.

3.2.1 Develop moisture induction methods

The parameters for developing moisture induction methods are based on theoretical models developed to predict warpage of unidirectional, anisotropic panels (Wood and Hanna 2020), (Wood 2019). The assumptions presented by the theoretical model are addressed for their relevancy to designing experimental moisture-induction methods.

To simulate an individual lamina from an LVL panel, Wood (2019) begins by designing his model as a two-dimensional, fibrous, anisotropic elastic plate. The plate has an aspect ratio of 1:2 with the long dimension, *2L*, representing fibers oriented parallel to the long, *x*-direction. The *L* dimension describes the transverse, *y*-direction. Panel thickness, *h,* is qualitatively described as $h << L$, because thickness is a programmable parameter in the model. Following the aforementioned constraints, a two-dimensional body is designed to mimic the behavior of a rectangular LVL panel. The schematic for the described plate is in Figure 3.2.1.

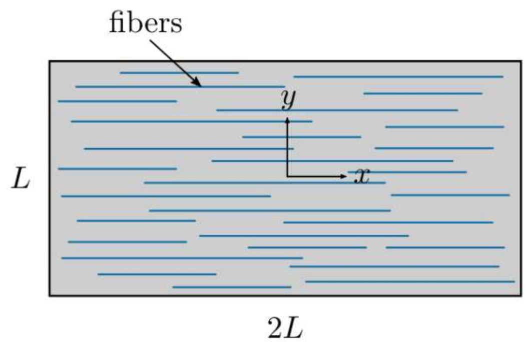

Figure 3.2.1: Diagram of anisotropic plate used for mathematical modeling (Wood 2019).

Experimental design parameters are obtained from the plate schematic. To begin designing the warpage experiments, veneers listed in Table 3.1.1 are cut on a bandsaw to a size of 7.5 x 15 inches to follow the theoretical model's aspect ratio. The plate schematic assumptions describe the two-dimensional nature of the specimen.

Next, the three-dimensional warpage behavior described by the model is explored. The model defines moisture gradients to vary along the *x*-direction with resultant warpage occurring the planar transverse, or *y*-direction (Wood 2019). With the moisture gradient varying across the long direction of the panel, the through-thickness moisture content is assumed to be consistent.

The restraints on the moisture gradient and warpage behavior on the dimensions of the plate provide guidance when designing experimental moisture induction methods.

The parameters of the model's warpage behavior provide guidance when designing moisture induction methods. With the swelling gradient only varying along the long, *x*-direction, when designing the wetting methods, applying moisture to both sides of the panel simultaneously is the technique used to follow this constraint.

To produce moisture-induced deformation, three wetting methods are introduced. Three tools are selected to induce moisture on veneers: damp sponges, damp paper towels, and a water spritzing bottle. The weight of the water introduced by the tools is measured to determine how much water is added by each wetting method. Each wetting method is shown in Figure 3.2.2 with a corresponding description of the procedure used to apply moisture to a veneer.

<table>
<tr><td>A: Damp Sponges
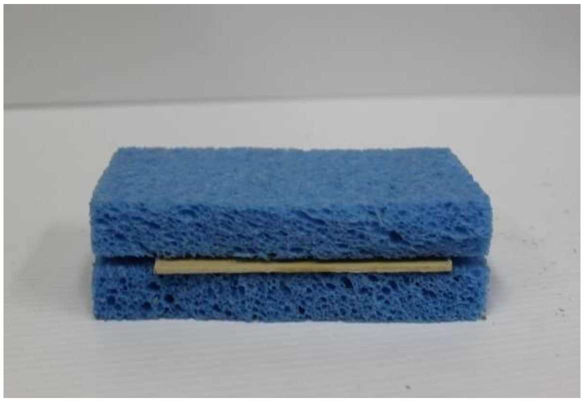</td><td>A small veneer sample is placed between two wetted, damp sponges for one minute. Sponges were rewet and rung out between samples to ensure consistent moisture.
The weight of water in the damp sponges is noted as 33.37 g after taking a difference in weight from the dry sponges.</td></tr>
<tr><td>B and C: “Spritz” Method
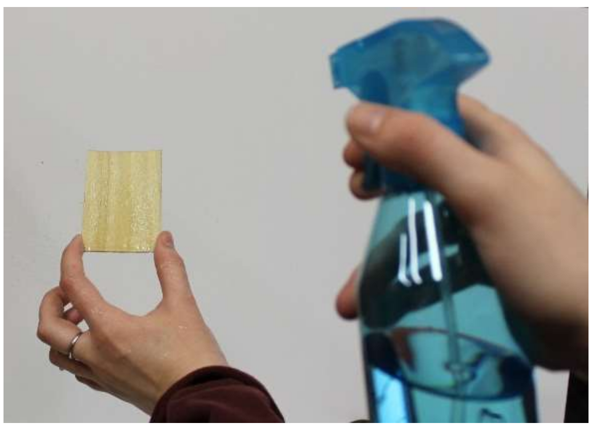</td><td>A spray bottle was used to “spritz” veneer from ~2 ft away. Both surfaces of the veneer were sprayed the same amount of times (1 or 5 spritz) in order to evenly wet the entire sample. The water weight from 2 spritz ≈ 1.6 g and 10 spritz ≈ 8.1 g.</td></tr>
<tr><td>D: Damp Paper Towels
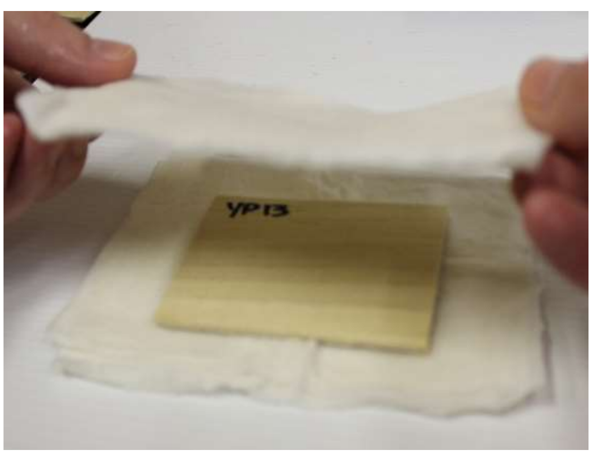
</td><td>Two damp Scott Rags paper towels are used to wet both surfaces of a veneer sample for one minute. Similar to the sponge method, the paper towels are rewet between samples to give same amount of moisture. The weight of water in the two wet paper towels is 45.87 g.</td></tr>
</table>

Figure 3.2.2: Photos and descriptions of moisture induction methods.

3.2.2 Evaluate moisture induction methods

Following development of the moisture induction methods, each method is measured for the exact amount of moisture added to a sample. To determine the moisture content change caused by each method, the moisture content before and after treatment is measured. Before the wetting method is applied, the weight of a small sample of veneer (~2 to 4 in^2) is measured on a balance sensitive to the 0.001 g decimal place. At this point, initial moisture content of the sample is measured by a J-2000 Delmhorst moisture content meter. This meter has a moisture range of 6-40%.

The accuracy of the Delmhorst moisture meter and E-15 attachment electrode is tested during the evaluation of the moisture induction methods. The moisture content measured by the meter is compared to the gravimetrically calculated moisture content to determine the accuracy and suitability of using the instrument in this project. During the quantification of the moisture induction methods, all five species of veneer listed in Table 3.1.1 are used, so the meter's resistance value is adjusted each time a new species was tested as specified by the manufacturer.

After the initial moisture content conditions are recorded, the moisture induction treatment is carried out. Immediately after the small veneer sample is treated with the intended moisture induction method, the weight of the sample post-treatment is recorded, and another moisture content measurement is taken with the moisture meter.

After the post-treatment conditions are recorded, the samples are placed in a laboratory oven set at 103°C for several days to be dried to a moisture content of 0%. At this point, the sample's oven dry weight is recorded. The gravimetric moisture content is calculated using Equation 1, as stated by ASTM D-4442 (2020), allowing moisture content to be determined at any point during the quantification procedure. Additionally, the gravimetric moisture content is compared to the moisture meter's readings to determine the meter's approximate accuracy. The results from quantifying individual moisture induction methods are presented in section 3.3.1.

3.2.3 Create moisture gradients

Using the results from quantifying individual moisture induction methods, the next step is to use a combination of the methods to create moisture gradients on veneers. The following procedure is a pilot study to create moisture gradients to be used in the warpage experiments. Two different moisture gradients are created that induce different moisture concentrations: one high and one low concentration gradient. Additionally, using the low concentration moisture gradient, the surface area of the applied wetting methods will be manipulated. The purpose of developing different gradients is to investigate the effect of moisture concentration on warpage behavior.

To begin designing moisture gradients, the individual wetting methods are combined on larger veneers. The theoretical gradient shown on the left in Figure 3.2.3 is digitally measured and converted to the dimensions of the experimental panel, as shown on the right. Each contour line in the moisture gradient defines a region. The center-most regions represent areas where higher moisture-inducing wetting methods will be applied. The outer regions of the moisture gradient represent areas where no moisture will be induced. The strategic placement of different moisture induction methods will allow for a gradient in moisture concentration throughout the veneer.

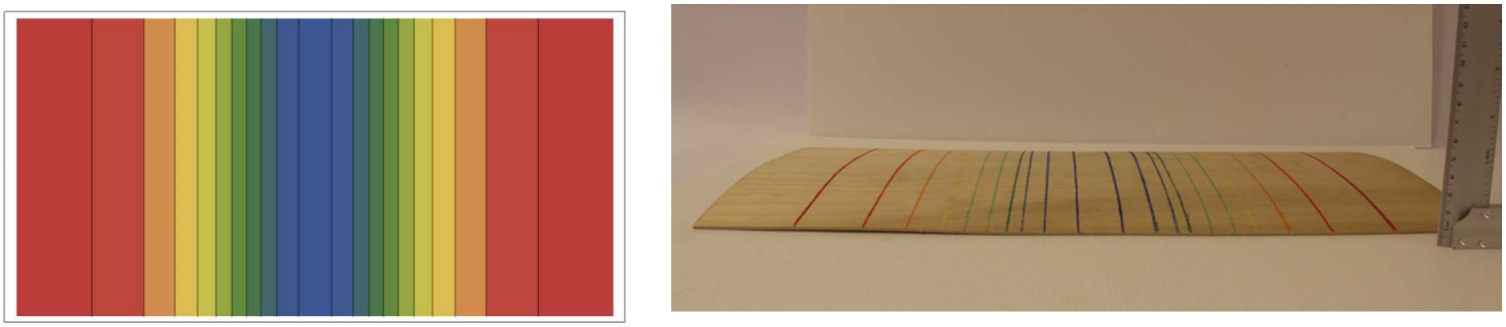

Figure 3.2.3: Theoretical moisture gradient scenario (Wood 2019) recreated on veneer.

The measurements for each region of the gradient on the bench-top sized panel is given in the Table 3.2.2 below. Due to the gradient's symmetry about the panel's center, only one side of the panel's dimensions needs to be determined. The dimensions in Table 3.2.2 will be the standard moisture gradient dimensions for all warpage experiments.

Moisture Gradient Dimensions

Region	**Location from Panel's Edge**
Region 1	1.875"
Region 2	3.125"
Region 3	3.96"
Region 4	4.583"
Region 5	5"
Region 6	6.413"
Region 7	5.83"
Region 8	6.042"
Region 9	6.458"
Region 10	7.08"
Center	7.5"

Table 3.2.2: Measured dimensions of the veneers' moisture gradient used in warpage experiments.

The moisture gradient dimensions are used to mark the areas for moisture induction treatment. In Figure 3.2.3, moisture is concentrated toward the center of the panel, so methods are selected to produce a moisture gradient with decreasing concentration toward the end of the panel. The moisture-induction treatment is conducted in tandem, targeting both surfaces of the panel, symmetrically about the panel’s center. The treatment used in the centermost regions (Region 8 to panel’s center) is five spritz from the spray bottle and Region 3-7 received the paper towel method. Regions 1 and 2 were left untreated to produce the low concentration end of the moisture gradient. The moisture-induced warpage of the veneer after 30 minutes is shown in Figure 3.2.4.

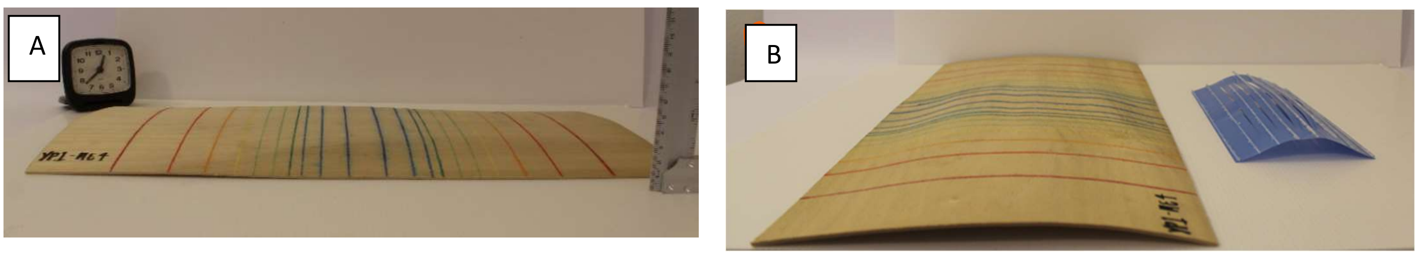

Figure 3.2.4: Deformation of the experimentally recreated swelling scenario.

When comparing the warpage produced by the experimental moisture gradient to the toy model created by Wood shown on the right in Figure 3.2.4(B), the geometries present similar axisymmetric shapes. The toy model has the center slits open from one another simulating middle expansion, illustrating the warpage behavior of the veneer (Wood 2019). As the moisture gradient is applied, the wood cells in the veneer’s center are swelling, causing overall expansion within the center region of the panel. The geometry of the toy model and warped veneer depicts a dome-like axisymmetric shape with ends resembling approximated cylinders.

Using the techniques developed to create a moisture gradient, the next step is to develop moisture gradients that produce different magnitudes of moisture concentration. The combination of wetting methods used in each concentration scenario is taken from the results testing the individual methods. The diagrams of the two gradients are shown in Figure 3.2.5 listing the wetting methods used in each moisture concentration scenario.

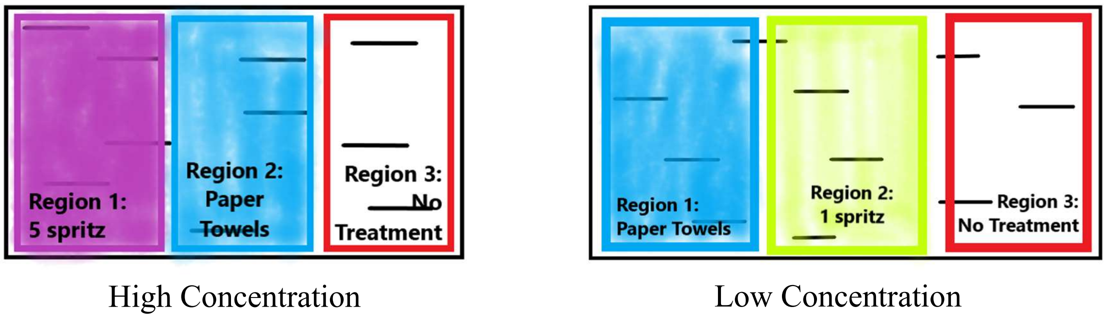

Figure 3.2.5: Diagrams of the methods used for the different moisture gradient concentrations.

In Figure 3.2.5, only one half of the gradient is used to establish a difference between low and high concentration gradients. When applying the moisture gradients to a full-sized sample, the gradient will be applied symmetrically about the panel's center, but the full gradient is not needed for determining a difference between the gradient's concentrations.

The high concentration moisture gradient, shown on the left of Figure 3.2.5, is designed with the wetting methods that induce the largest amount of moisture content change. The 5 spritz method is used on the high concentration gradient as this technique induces the greatest amount of moisture. Paper towels and a region of no treatment is also used in the high concentration gradient. To produce the low concentration moisture gradient shown on the right of Figure 3.2.5, paper towels and the 1 spritz wetting methods are applied next to each other following a region of no treatment.

A set of experiments is conducted to determine a moisture gradient's change in moisture concentration across the surface of a panel. Three regions are marked off to identify the wetting method it receives. Treatment is applied, and a moisture content reading is taken in each region. The overall gravimetric moisture content of the sample is also calculated throughout the experiment using Equation 1 presented in Section 2.2. Figure 3.2.6 illustrates the experimental set up for the low concentration moisture gradient. The photo is taken after the treatment is applied.

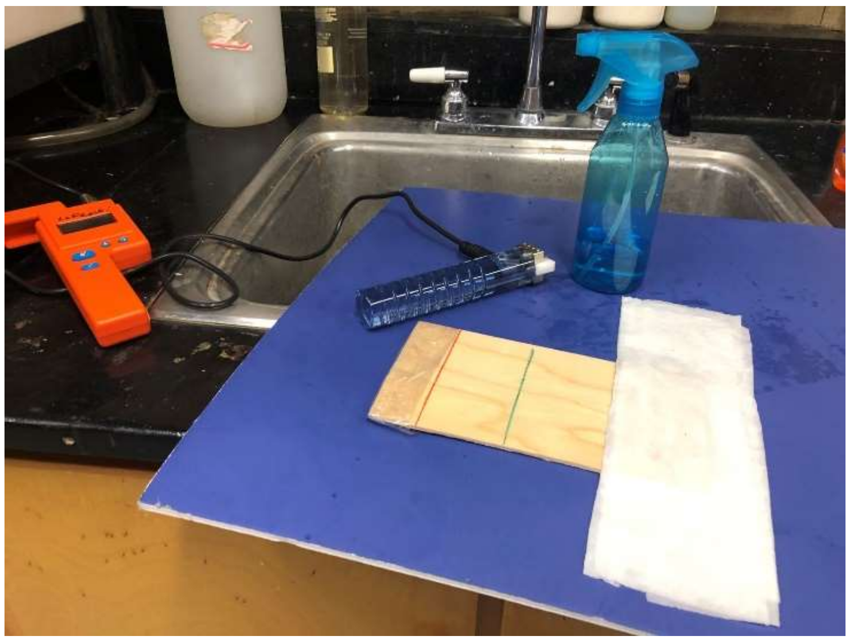

Figure 3.2.6: Experimental set up to create moisture gradients.

The order of the moisture induction methods applied to a sample is determined based on results from evaluating each wetting method. In Figure 3.2.6, plastic film is applied to the region receiving no treatment to keep this region of the sample dry while wetting methods are applied. The wetting methods that are applied to induce moisture follow the protocol outlined in the descriptions of the methods in Figure 3.2.2. The middle region of the sample received 1 spritz to both surfaces of the veneer while the last region received moisture from damp paper towels applied for 1 minute. Immediately after treatment, moisture content was measured with the same moisture meter and attachment electrode and a final weight of the sample is recorded. Ten samples of the low concentration gradient are conducted and 6 are conducted for the high concentration gradient. The sample sizes are small because only a differential in moisture content across the sample is needed to be determined in this stage. Results from the development of moisture gradients are presented in Section 3.3.2. The moisture gradients are quantified for the global change in moisture content induced during the warpage experiments in Section 3.3.3. The samples used in the warpage experiments are given in Table 7.1.1.

Manipulating the surface area of the applied moisture gradient is also a variable of interest during the warpage experiments. The manipulations made in this experiment are to half and double the dimensions from Table 3.2.2 to create moisture gradients that cover different areas on a panel's surface. Figure 4.3.3 shows a photo of the three different sized moisture gradients where the surface area of moisture gradients increases from left to right.

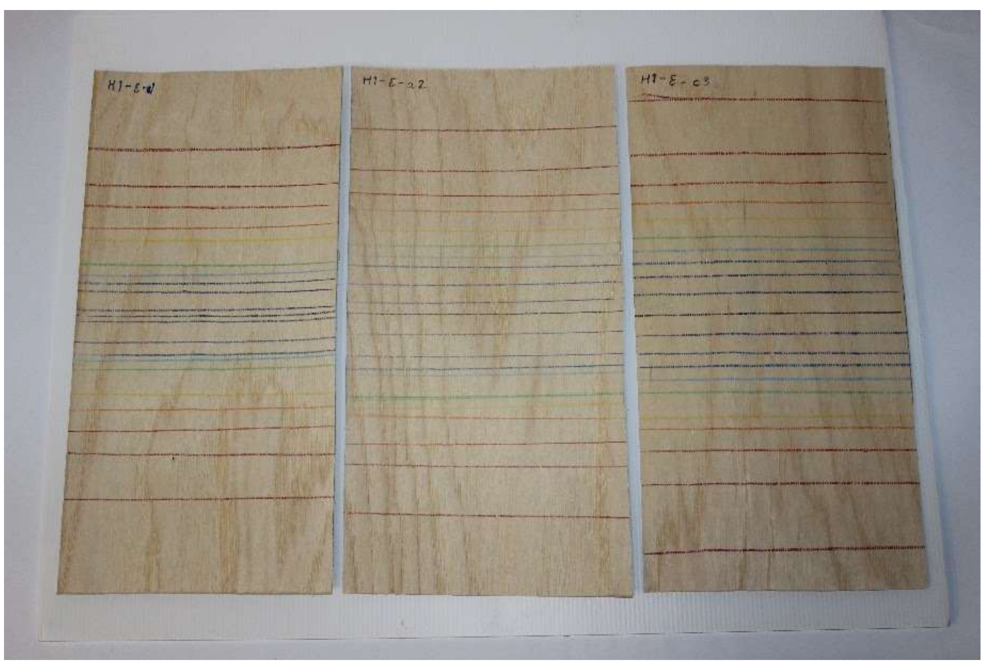

Figure 3.2.7: Surface area manipulations of applied moisture gradients. The left sample has the smallest applied moisture gradient area. The center sample follows standard surface area for moisture application. The right sample has the largest area of applied moisture.

In Figure 3.2.7, the size in area allowed for center moisture induction increases in the panels from left to right. Closer spaced lines indicate higher moisture concentration compared to wider spaced lines. Changes in the applied gradient's surface area and concentration of the moisture gradient are used in Chapter 4 warpage experiments to determine the effect each manipulation on warpage behavior.

3.3 Results and Discussion

The results for the first objective are presented in the previous section. The first objective aims to provide quantifiable methods for producing moisture-induced warpage in wood. To quantify the methods and analyze their repeatability, three sets of results are provided:

- Quantification of individual moisture induction methods
- Quantification of moisture gradient scenarios
- Analysis of moisture gradient quantification procedure

3.3.1 Quantification of individual moisture induction methods

An experiment is conducted to determine how much moisture each wetting method adds to a sample. The value of interest, the moisture content differential, is calculated by taking the difference between the initial and post-treatment moisture content. The change in a sample's gravimetric moisture content compared to the meter reading is plotted in Figure 3.3.1.

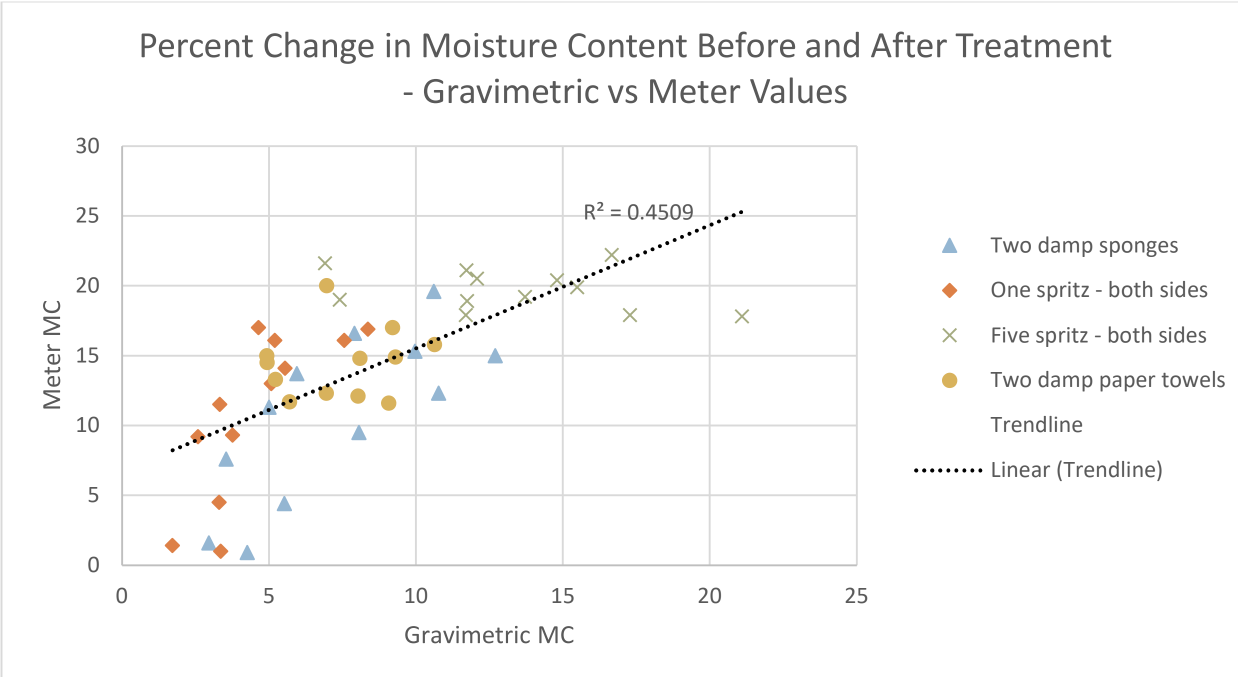

Figure 3.3.1: Scatter plot showing the relationship between moisture content differentials for the calculated, gravimetric moisture content vs meter read value.

This data set includes the 48 treated samples from the individual wetting method observations. The 48 samples used for the moisture content meter tests consist of 12 samples from each of the five different species (hickory, yellow-poplar, red oak, southern yellow pine, and Douglas-fir). Each species was used in each wetting method test to determine the average percent change in moisture content each method induces.

The overall R^2 value for the set of tests was 0.451 indicated a mediocre relationship between the differentials in moisture content between the gravimetric and meter-read moisture content. The data in the 0-5% change range that outlies from the rest of the data set can be explained due to the moisture meter's inability to read in this range. The moisture meter has a range of measuring moisture content from 6-40%.

In the scatter plot that displays all the data from this experimental trial (Figure 3.3.1), the methods are differentiated to see which methods cause larger moisture differentials. The method that induces the largest change in moisture content out of the four methods is the 5 spritz method, indicated in the graph by X's. By examining the results, methods are selected to be used to measure experimental moisture gradients.

To analyze the accuracy of the moisture meter, the gravimetric moisture content and meter read values are compared by method. In Figure 3.3.2, moisture content differential data is presented by method to show the relationship between gravimetric and meter-read moisture content.

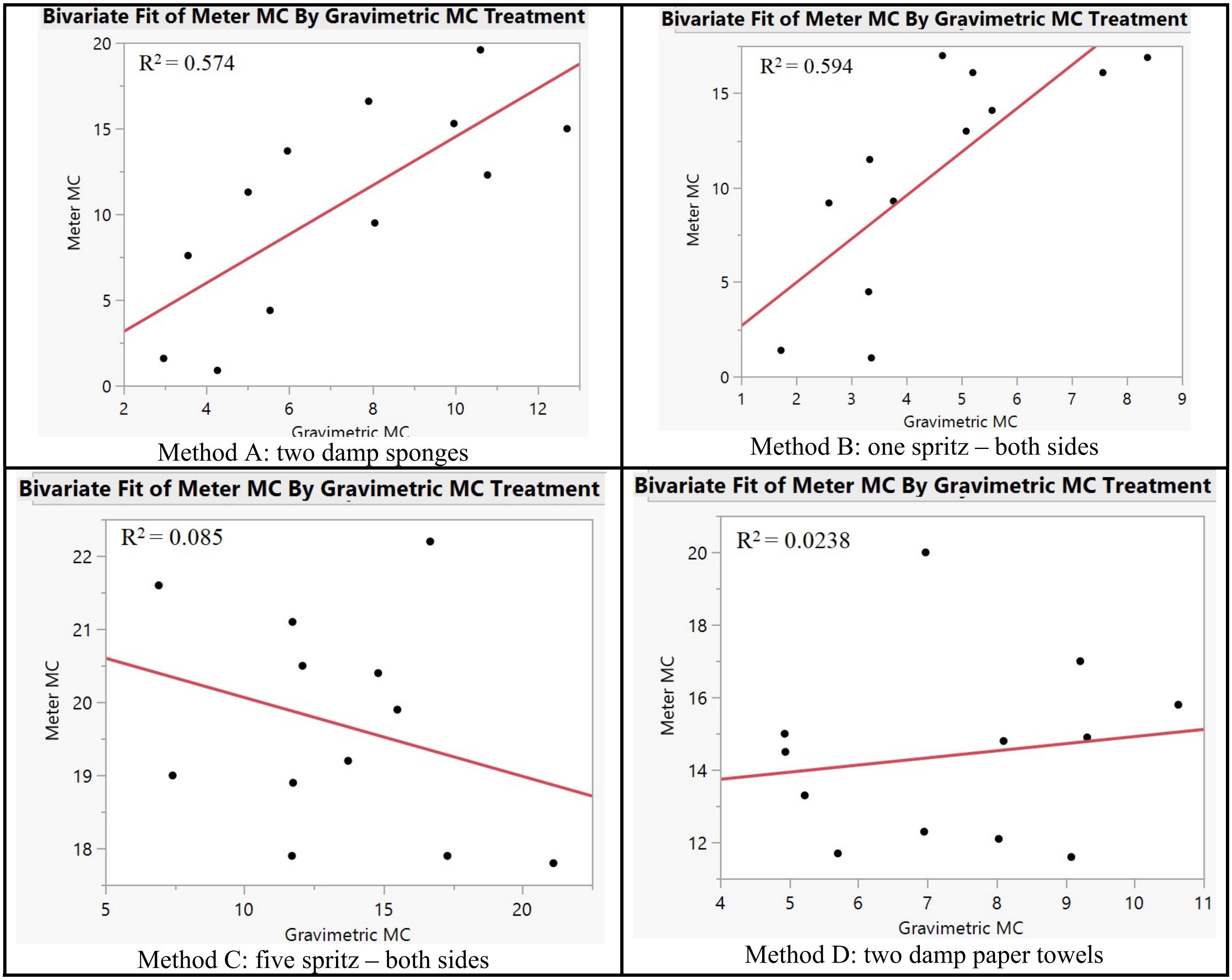

Method A: two damp sponges

Method B: one spritz – both sides

Method C: five spritz – both sides

Method D: two damp paper towels

Figure 3.3.2: Graphs showing the relationship between gravimetric (predicted) and meter-read (measured) moisture differentials for the four methods.

By displaying the data separately, the individual graphs in Figure 3.3.2 imply the consistency of each method. Linear regression is used to determine a relationship between the two variables. The R-squared (R^2) value is used to give a percentage of the variance in the dependent variable, explained by the independent variable. The closer the R^2 value is to 1, the stronger the correlation between the variables.

As shown in Figure 3.3.2, Method A and B have the most positive correlation between the meter and gravimetric moisture content method with R^2 values of 0.574 and 0.594 respectively. Although Method C resulted in the highest moisture content differentials, this graph shows a poor (R^2 = -0.085) relationship between the predicted and measured moisture content. This is attributed to the meter's inability to measure above 40% moisture content because some wetting methods add enough moisture to exceed the meter's upper threshold.

When considering the accuracy of the moisture meter overall, Figure 3.3.2 gives some insight into how the E-15 electrode performed. Overall, there is a moderate correlation with an R^2 value = 0.451 as seen in Figure 3.3.2. The relationship between the calculated, gravimetric moisture content and the moisture content recorded from the moisture meter is considered moderate. From this data analysis, limitations concerning meter-read moisture content measurements are present, therefore the gravimetric moisture content calculation method is used during the Chapter 4 warpage experiments.

3.3.2 Quantification of moisture gradient scenarios

The results in the following section present the data collected during development of experimental moisture gradients. The procedure to measure each region's moisture content is presented in Section 3.2.2. Two moisture gradients are developed: one high and one low concentration. Each region of the moisture gradient is measured by a moisture meter for the moisture content induced by the applied wetting method. The results for the low concentration gradient is presented in Figure 3.3.3.

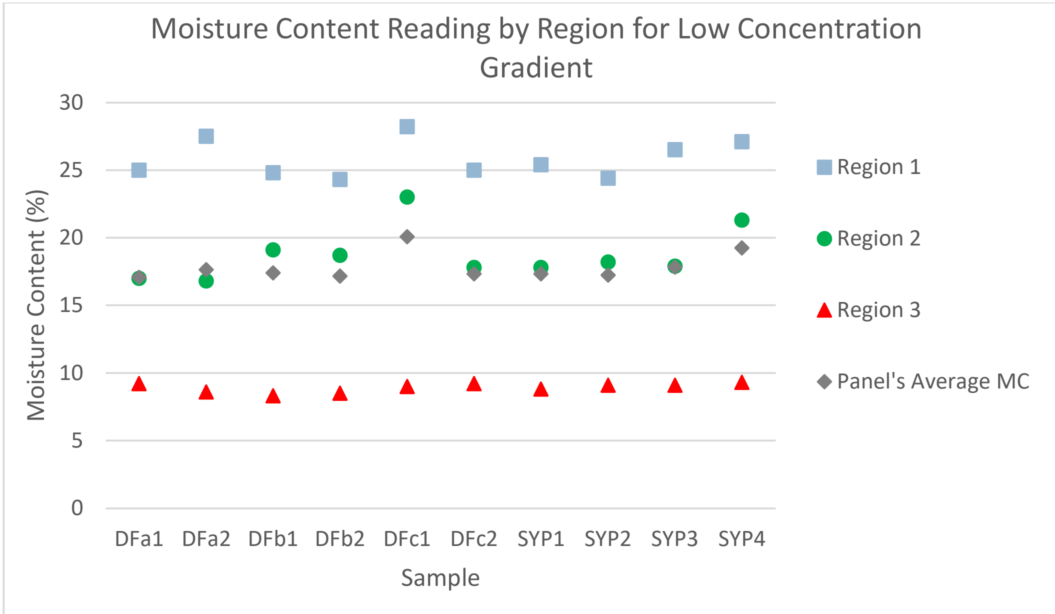

Figure 3.3.3: Recorded values from the moisture meter after treatment for each region in the low concentration gradient.

In the low concentration gradient, region 1 received damp paper towels, region 2 received 1 spritz to both sides and region 3 received no treatment. In the high concentration gradient, region 1 received 5 spritz to each side, region 2 received damp paper towels and region 3 received no treatment. The results of the moisture content reading by region for the high concentration gradient is shown in Figure 3.3.4.

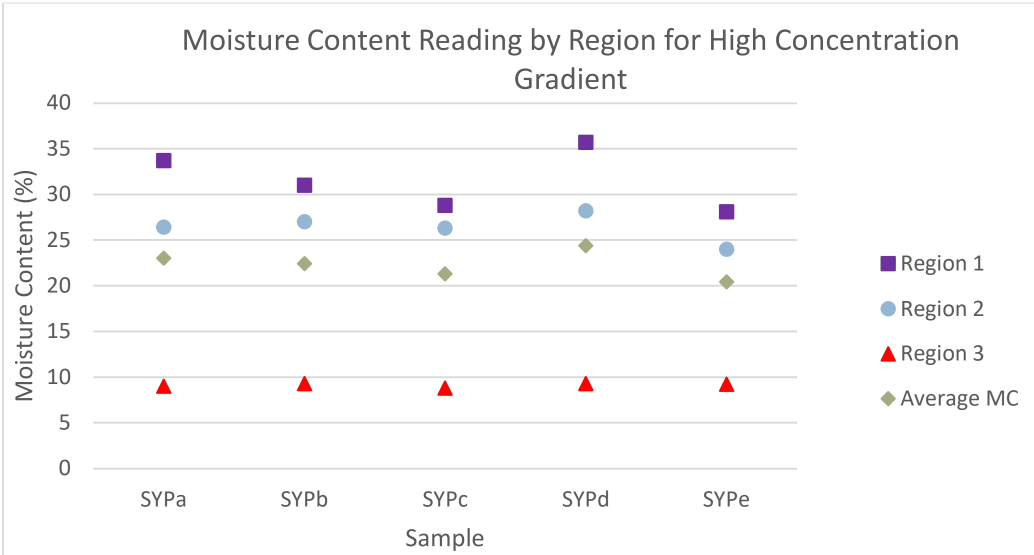

Figure 3.3.4: Recorded values from the moisture meter after treatment for each region in the high concentration gradient.

After recording the moisture content of each treatment region after moisture induction, an average of the three regions was calculated to determine an overall average moisture content for the sample. The average moisture content for each gradient experiment is indicated by the diamonds in Figures 3.3.5 and 3.3.6. The average moisture content for the low concentration gradient is 17.83% and the high concentration gradient is 22.32%.

To investigate the accuracy of the moisture meter, the average moisture content for each moisture content gradient is plotted against the calculated gravimetric moisture content. The comparison of the average moisture content from the two different gradients is shown in Figure 3.3.5.

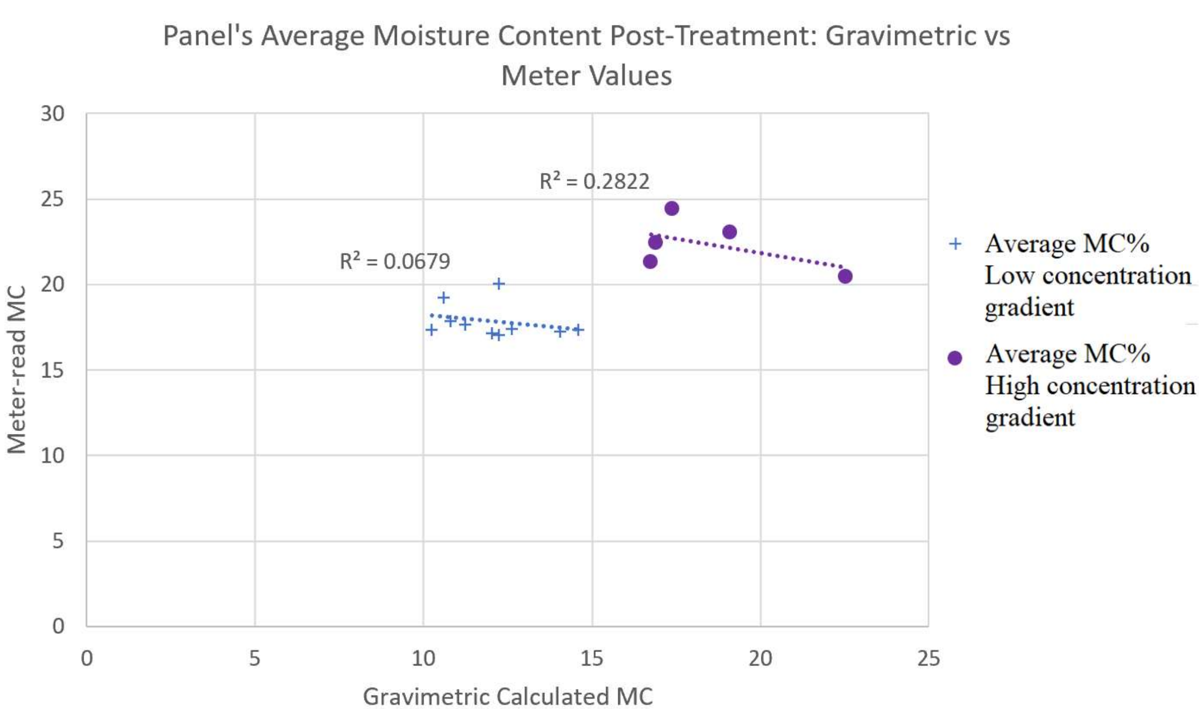

Figure 3.3.5: Comparison of the gravimetric moisture content against the average moisture content read from the meter by moisture gradient. The high concentration gradient values are circles, and the low concentration values are crosses.

In Figure 3.3.5, the two clusters of points correspond to the two moisture gradients. The high concentration gradient intended to induce a greater amount of moisture content change is represented by circles and the low gradient is represented by crosses. The high concentration gradient has a higher average than the low concentration gradient. The two gradients are used in the chapter 4 warpage experiments to see the effect of moisture gradient concentration on deformation. The moisture meter, however, is not used later in the experiment. The moisture meter was helpful to establish a difference in concentration of the wetting individual methods. After creating moisture gradients using a combination of methods, the gravimetric moisture content will be used to quantify the global moisture content change induced by the moisture gradients used in the warpage experiments.

3.3.3 Analysis of moisture gradient quantification procedure

One of the main objectives for this research study is to provide quantifiable moisture induction methods to create experimentally controlled warpage. In this section, the two moisture gradient scenarios designed to produce variation in moisture content magnitude are analyzed for how much moisture each scenario adds to a sample during the warpage experiments in chapter 4. The summary statistics for the moisture content data for each concentration scenario are given in Table 3.3.1.

Low Concentration	Post-Treatment MC	Initial MC	Δ% MC
Average	6.96	3.54	3.42
Standard Deviation	3.29	1.42	2.50
CoV	47%	40%	73%
High Concentration	Post-Treatment MC	Initial MC	Δ% MC
Average	10.13	3.40	6.72
Standard Deviation	3.99	0.94	3.71
CoV	39%	28%	55%

Table 3.3.1: Summary statistics for the moisture gradient concentration data obtained from warpage experiments.

Listed in the summary statistics Table 3.3.1, the average change in moisture content takes the difference between the post-treatment and initial moisture content measured for each sample. The average change in moisture content for the low concentration moisture gradient scenario is 3.42% and is 6.72% for the high concentration moisture gradient. The raw data from the warpage experiments is presented in Appendix A. This data from the warpage experiments using different moisture gradient concentrations is visualized in Figure 3.3.6.

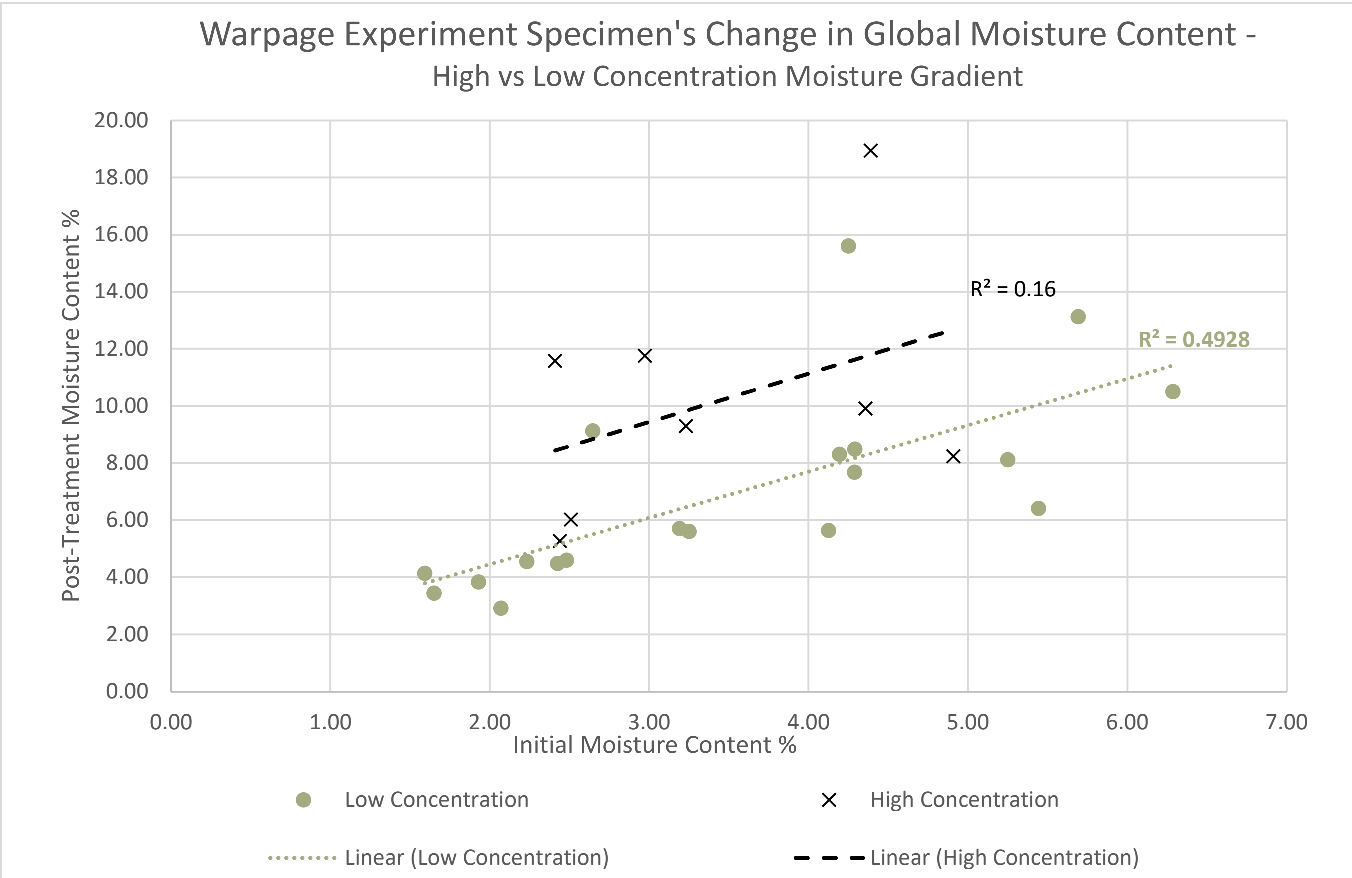

Figure 3.3.6: Change in a sample's moisture gradient before and after moisture-induction treatment plotted by moisture concentration gradient.

In Figure 3.3.6, each moisture gradient concentration warpage experiment is plotted with initial moisture content value against the post-treatment moisture content. The data is differentiated by the two designed moisture gradient scenarios used during the experiments. The high concentration gradient, represented by X, has an R^2 value of 0.160 whereas the lower concentration gradient represented by dots has an R^2 value of 0.493. The reported values show that positive correlation does exist in both moisture gradient scenarios. The lower concentration gradient has a stronger correlation which could be attributed to the group's larger sample size.

To determine the statistical significance of a moisture gradient's effect on changing the global moisture content of a sample, two-tailed paired t-tests are conducted on Excel. The values for the tests are obtained by determining the average change in moisture content for each moisture gradient concentration scenario, as reported in Figure 7.1.1 of Appendix A. The first set of t-tests to run with this data is a comparison among the average moisture content before and after treatment for each moisture gradient scenario.

A paired, t-test is conducted using the values from initial moisture content ($\mu_{\text{Initial MC}}$) and the post-treatment moisture content ($\mu_{\text{Post-Treatment MC}}$) to see if the treatment has an effect on the change in overall moisture content. The null hypothesis (H_0) for this case states the average moisture content for each group is the same whereas the alternative hypothesis (H_a) states the averages differ. The arguments for analyzing the statistical significance between the initial moisture content and post-treatment moisture content are given below:

$$H_0 = \mu_{\text{Initial MC}} = \mu_{\text{Post-Treatment MC}}$$

$$H_a = \mu_{\text{Initial MC}} \neq \mu_{\text{Post-Treatment MC}}$$

Two separate t-tests are conducted for each moisture gradient concentration scenario. The results are presented in Appendix B. In both cases, the treatment methods for each moisture gradient scenario proved to provide a statistically significant change in overall moisture content. Table 7.2.1 presents the results for the t-test on the lower concentration moisture gradient. The two-tailed p-value of $1.73\text{x}10^{-5}$ is significantly smaller than the significance value of 0.05, rejecting the null hypothesis. This is the same for the higher concentration moisture gradient scenario; as reported in Table 7.2.2, the null hypothesis is rejected since the p-value (0.00199) is less than the 0.05 significance value.

After analyzing the statistical significance of each case, the next step is to compare the populations of the two moisture gradient scenarios to each other. The average change in moisture content for low concentration gradient (μ_{Low}) is compared to the high concentration gradient

(μ_{High}) to see if the average change in moisture content for each moisture gradient is statistically significant. For this analysis, a paired, two-sample t-test assuming unequal variance is conducted. The unequal variance case is selected because the variances and standard deviations between the two groups is not assumed to be equal. The arguments for this case are stated below:

$$H_0 = \mu_{\text{Low Change in MC}} = \mu_{\text{High Change in MC}}$$

$$H_a = \mu_{\text{Low Change in MC}} \neq \mu_{\text{High Change in MC}}$$

The output from the t-test is presented in Table 7.2.3 of Appendix B. From these results, the statistical significance of each moisture gradient scenario is confirmed. With a two-tailed p-value of 0.03, this value is less than the significance value of $\alpha = 0.05$. In this case, the null hypothesis is rejected meaning that the average change in moisture content for the two methods is different enough from each other to prove statistical significance. In conclusion, the high and low moisture gradient scenarios do produce an overall change in moisture content that qualifies the developed methods to produce moisture gradients of varying magnitudes.

4.0 Measuring Moisture-Induced Deformation

The second objective is to investigate and develop methods to measure moisture-induced deformation of veneer specimens. This chapter presents methods, techniques, results, and discussion for measuring warped shape changes. The method to produce moisture gradients developed in objective one is used to induce warpage and subsequent deformation is analyzed in this chapter. The result of objective two is the presentation of a specimen's warped geometry caused by variation in moisture gradient.

The flowchart in Figure 4.1.1 outlines the procedures and methods used to complete the second objective. Three subobjectives are developed. The first subobjective is to develop a qualitative deformation monitoring procedure to obtain an initial visual observation of the wetting methods. In this subobjective, time-lapsed photos are produced to show the magnitude of warpage over time. The visual observation provides a qualitative confirmation of warped deformation for each wetting method.

In the second subobjective, several deformation measurement procedures are explored, and 3D scanning technology is selected for use in this project. A procedure using a structured light scanner is developed to measure warpage on wood veneers. After calibration, the scanner is used to make 3D scans of warped specimens to analyze the effect of moisture induction methods.

In the third subobjective, warpage experiments are conducted to determine the effect of manipulations in a veneer's moisture gradient on warpage. The experimental variables selected are veneer thickness, moisture gradient concentration, and surface area. During each experiment, warped surface geometries are analyzed through a three-step data collection and conversion process, further outlined by Figure 4.2.5. A technique called curvature comb analysis is used to analyze the curvature profiles of the warped specimens. The effect of moisture gradients on surface geometries are compared to demonstrate each experimental variable's influence on warpage.

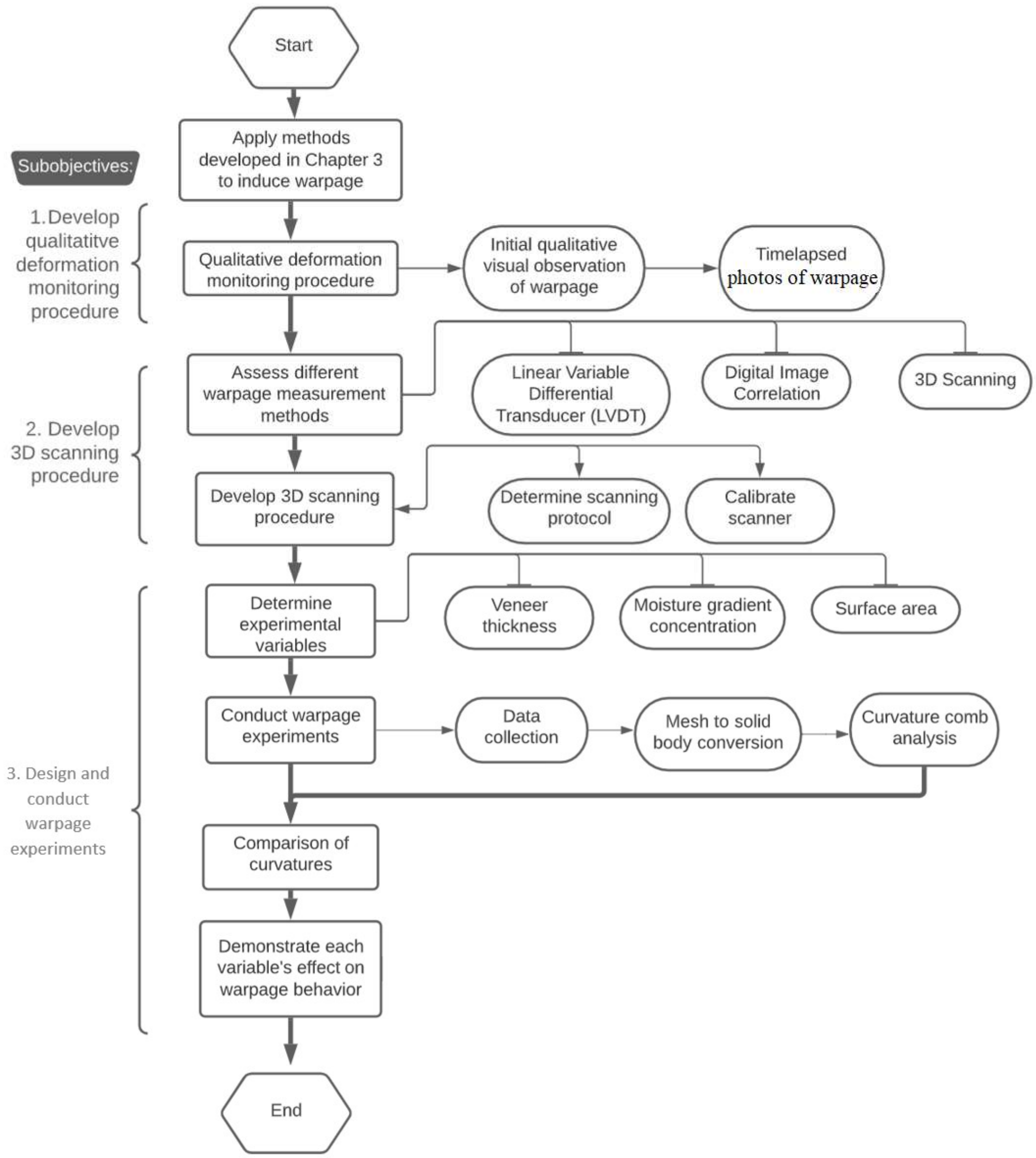

Figure 4.1.1: Flow chart outlining subobjectives for Objective 2.

4.1 Materials

The second objective is to develop a warpage monitoring method to measure the geometrical shape changes of moisture-induced wood deformation. The technology selected to measure experimental warpage is a handheld 3D structured light scanner, the EinScan-Pro. The principles of 3D scanning are discussed in Section 2.6.

During a scan of a veneer's surface, the scanner is connected to a computer that reconstructs and presents the collected surface profile data. The computer must have powerful graphic capabilities, so a new Lenovo IdeaCentre T540 desktop system was purchased for this project based on the minimum requirements stated by the 3D scanner's manufacturer (SHINING3D). The computer has an Intel Core i5 processing system with an NVIDA GeForce GTX 1660 Ti graphics card. Figure 4.1.2 shows a demonstration of the 3D scanning procedure with captions explaining everything used to make a scan. As the scanner projects lines on the warped veneer, the surface points are triangulated and reconstructed on the monitor of the computer.

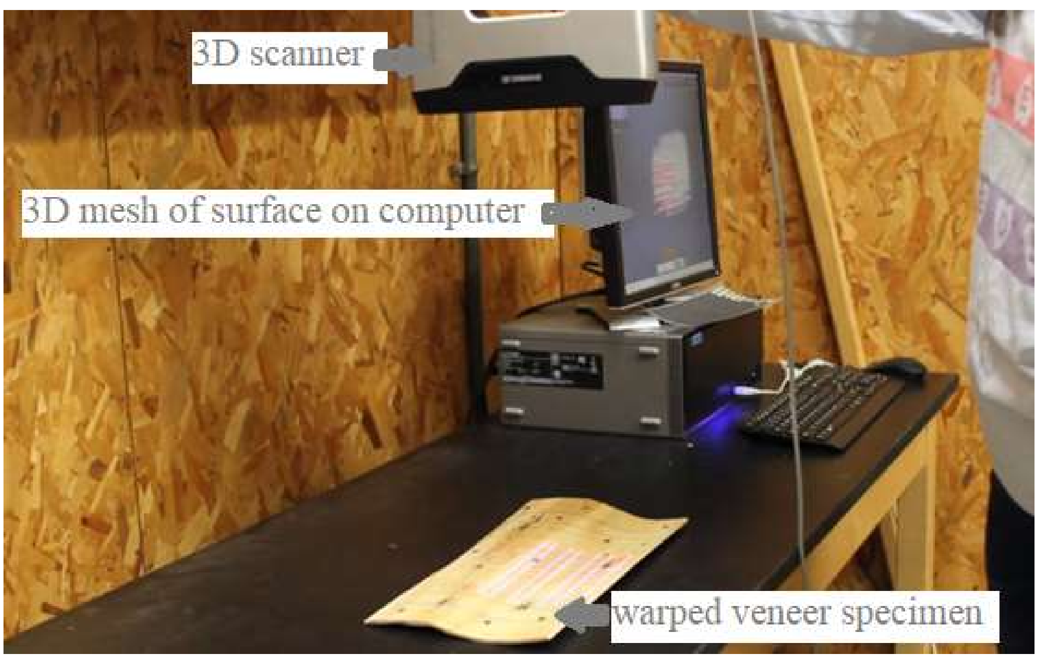

Figure 4.1.2: Three-dimensional scanning set-up.

To analyze the data collected by the EinScan-Pro, additional computer software is required. Computer Aided Design (CAD) programs such as SolidEdge (Siemens PLM 2021) and Autodesk Inventor (Autodesk 2021) are utilized for the powerful graphic processing tools they possess. The procedure to analyze 3D scan data utilizing the selected CAD programs is outlined in Figure 4.2.5.

4.2 Methods

Using the moisture induction methods developed during objective one, the next step is to create a method to monitor experimentally created, moisture-induced deformation. To achieve this, the EinScan-Pro 3D scanner is used to collect deformation data and Computer Aided Design programs are introduced to analyze the surface deviations of warped specimens. Development of this warpage monitoring method, or the second research objective, will be discussed in this next section.

The second objective is broken up into three subobjectives that are required for the development of a procedure to monitor warped shape changes in wood. The following subobjectives are discussed for the methods involved:

- Develop qualitative deformation monitoring procedure
- Develop 3D scanning procedure
- Design and conduct warpage experiments

Section 4.3 discusses the results from the warpage experiments. A set of experiments using the methods developed in chapter 3 are used to investigate the effect of different moisture gradients on warpage behavior.

4.2.1 Develop qualitative deformation monitoring procedure

During the development of moisture induction methods, qualitative methods for monitoring warpage are explored. A procedure is developed to monitor warpage over time by making time lapsed photographs. After placing a wet paper towel on the dry, flat veneer, using a digital camera set on a timer, a picture is taken every 30 seconds for the duration of 1 hour. An analog clock is included in the photos to show time passing. The 120 photos are strung together to create an approximately 90 second video showing the panel warping over the hour. Figure 4.2.1 shows photos from the beginning and end of the process.

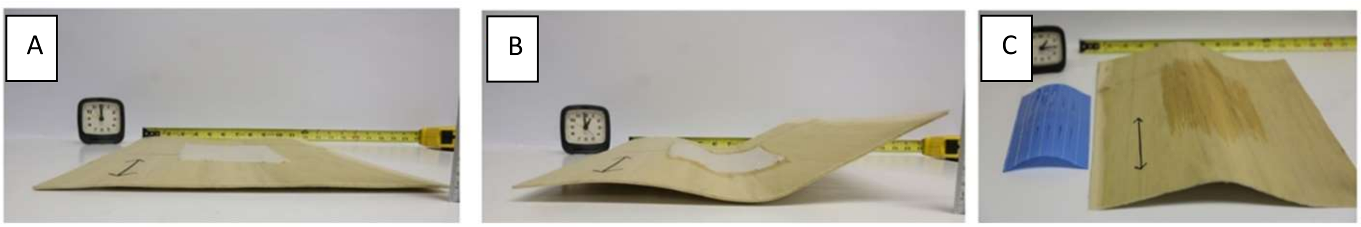

Figure 4.2.1: Photographs from qualitative monitoring of moisture-induced deformation.

In Figure 4.2.1, initial panel flatness at minute zero is seen in (A) and the final position of the warped yellow-poplar veneer is seen in (B) and (C). The deformation monitoring procedure allows for the qualitative confirmation of the moisture induction methods that are being explored. As shown in Figure. 4.2.1, early experiments are conducted by applying a wet paper towel on one side of a dry veneer's surface. Soon thereafter, however, it was realized that this one-sided moisture induction method is not congruent with the moisture gradients described in the models, and this change is accounted for. The qualitative deformation monitoring procedure, however, remains consistent throughout the rest of the experiments when additional documentation is needed.

The qualitative deformation monitoring procedure is used during the development of the wetting methods. In the following set of moisture induction experiments, the four methods are tested separately on hickory cut on a bandsaw to a size of 4x8”. Time-lapse photos are taken every 15 seconds to see deformation occur over 30 minutes. Figure 4.2.2 shows the results of the four samples side-by-side, labeled by method.

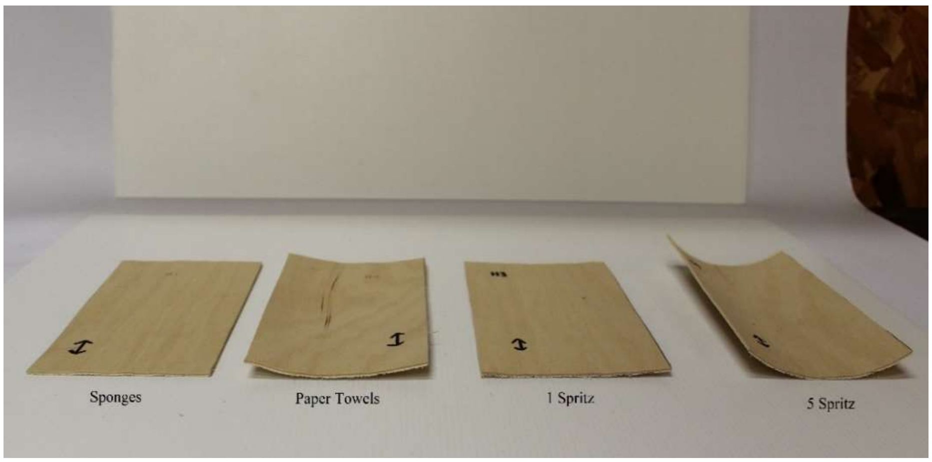

Figure 4.2.2: Four different wetting methods showing qualitative deformation after 30 minutes. Methods from left to right are: sponges, paper towels, 1 spritz, 5 spritz.

In Figure 4.2.2, moisture rom this round of testing moisture induction methods, the qualitative deformation monitoring procedure demonstrates the different methods cause differing magnitudes of warpage. The sponges and one spritz methods cause the least amount of warpage, followed by the paper towel method where there is some visible deformation. The five spritz method causes the most amount of observed warpage in this experimental trial. The observable deformation helps confirm the results quantifying each method in Chapter 3.

4.2.2 Develop 3D scanning procedure

The technique for measuring wood deformation in this experiment is based on 3D scanning technology. The operating procedure for the scanner has been outlined in Chapter 2's section on literature pertaining to measuring the surface deformation of wood panels. Using the manufacturer's instructions, a procedure for measuring the warpage of veneers using a 3D scanner is developed.

While operating the scanner, the scanning program's user interface helps guide the user through the process. Before making any surface measurements, the scanner is calibrated in a multiple step process. Two rounds of calibration are required to align the camera: 1) calibrating the scanner's distance from the object's surface, and 2) a calibration of the scanner's HD settings. After calibration is complete, the scanner is ready to make surface scans of the veneers.

To begin the surface measurement collection procedure, the HD handheld scan mode is selected in the scanning interface. In this mode, the scanner relies on small, reflective surface marker points applied to the specimen to aid in alignment during surface measurements. The marker points are seen randomly dispersed on the veneer sample in Figure 4.2.3.

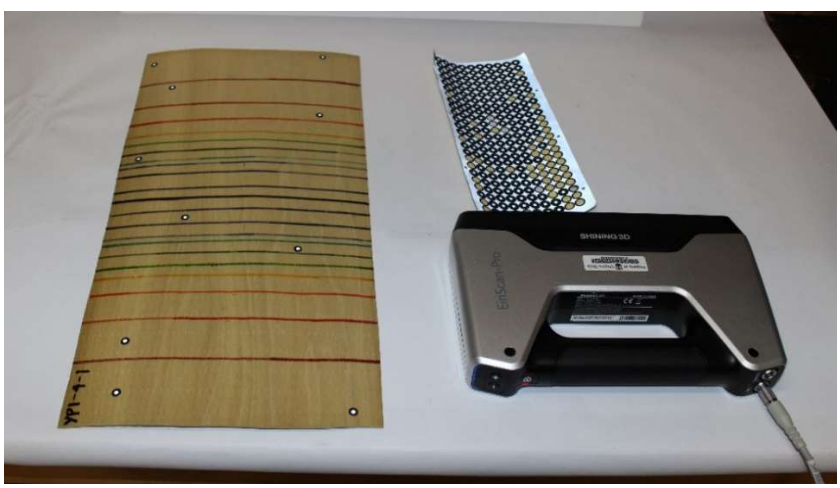

Figure 4.2.3: A sample of yellow-poplar veneer with the EinScan-Pro.

After a surface scan is completed, the software generates a rendering of the data points to reconstruct the object digitally, also known as a point-cloud or mesh. After a scan is completed, the 3D scanning software provided by Shining3D, the manufactures of the EinScan-Pro, produces a mesh reconstructing the scanned data. An example of a 3D rendering of scan data is shown in Figure 4.2.4.

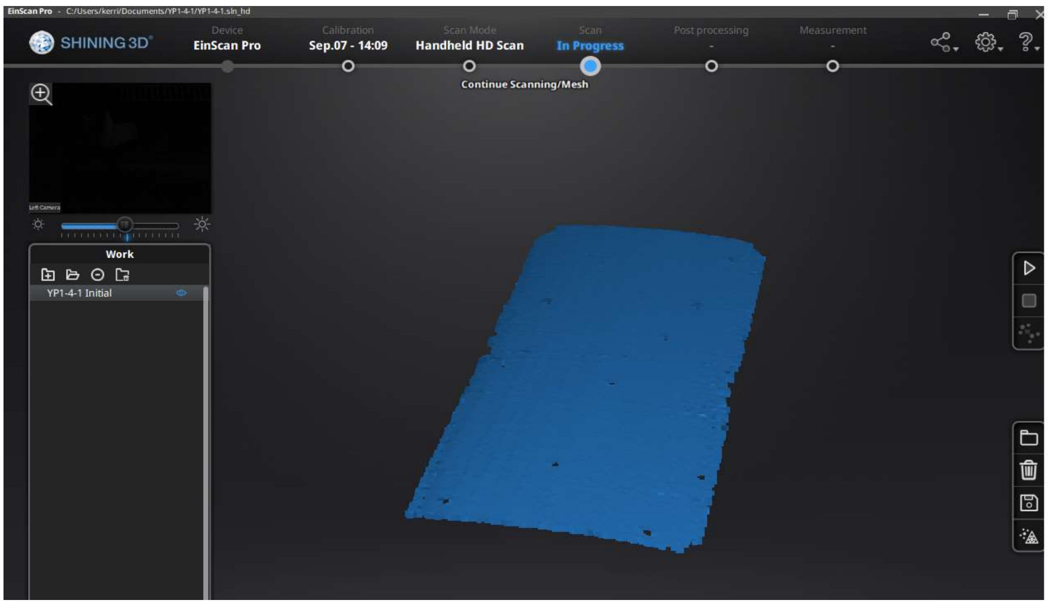

Figure 4.2.4: The EinScan-Pro scanning software interface.

As a scan is being completed, the three-dimensional point cloud is rendered in the computer, by the scanning software. As seen in Figure 4.2.4, the reflective marker points are the empty dots across the mesh's surface. The empty dots of data are automatically filled in when the scanning software exports the final mesh. The ability to automatically reconstruct missing data based on nearby collected scan data is a powerful feature included in the Shining3D scanning software interface.

The final mesh is exported to a third-party inspection software program (Siemens PLM Software 2021) where a 3D image, or "model" representing the data is generated. Additional steps are required to transform the scanned mesh data into a solid body that can be analyzed for surface deviations. In a CAD program, the solid body representing the surface scan data is analyzed and compared to other generated bodies produced using the same variables. The procedure to analyze 3D scan data is provided in the next section.

4.2.3 Design warpage experiments

Following the development of the procedure to collect surface profiles using the 3D scanner, methods to analyze surface profiles during warpage experiments are investigated. Warpage experiments using the methods developed in chapter 3 are designed to investigate the effect of a moisture gradient on resultant deformation. The three-dimensional scanning procedure developed in the last section is applied to reconstruct the surface geometry of each warpage experiment specimen.

Presently, there is no automatic process for obtaining geometry or deformation data on a 3D scanned object. The 3D mesh reconstructed by the scanning program is a visualization of the scanned object and has arbitrary dimensions. Prior to analysis of a specimen's warped surface, further manipulation of the collected scan data using Computer Aided Design is required. The flowchart in Figure 4.2.5 outlines the data conversion procedure to analyze warpage.

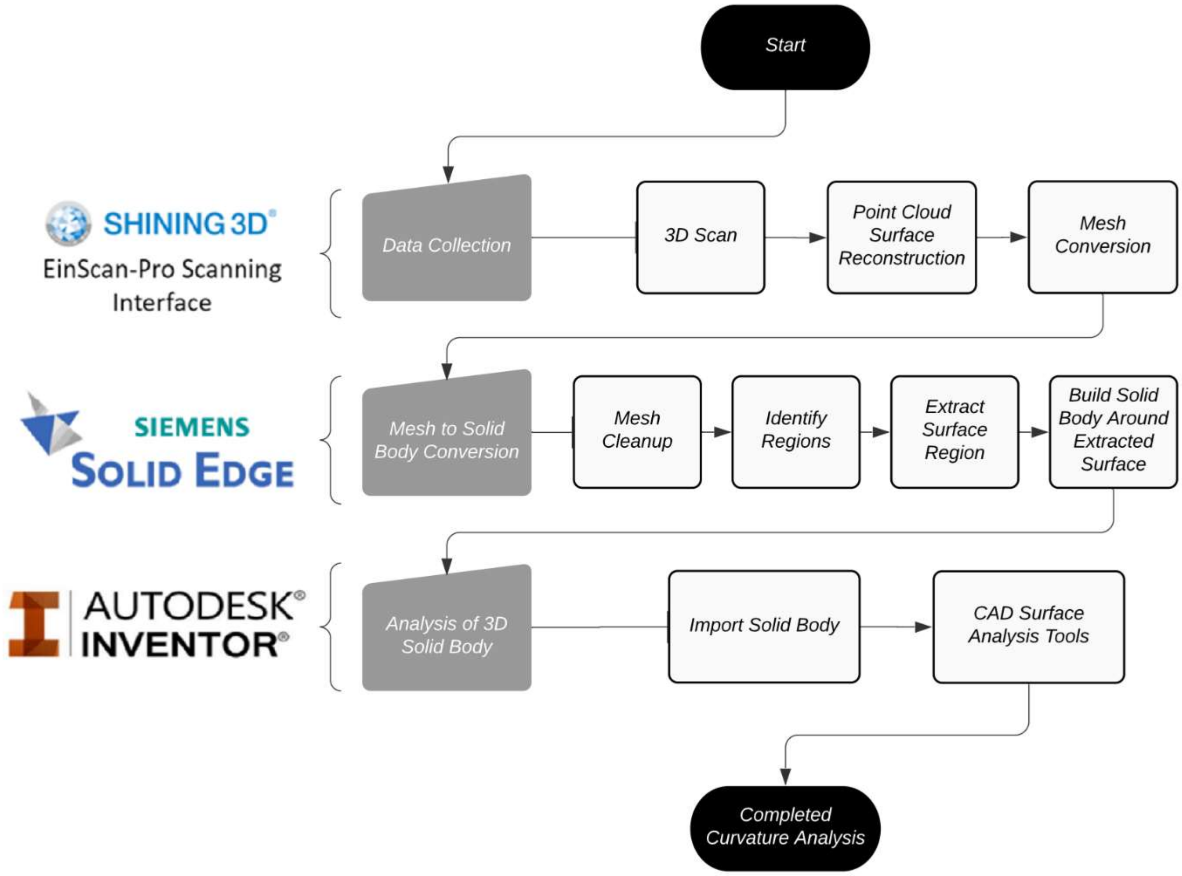

Figure 4.2.5: Flowchart outlining 3D scanner data collection and analysis procedure.

There are three steps in the 3D scanner data collection and analysis procedure: 1) data collection, 2) mesh to solid body conversion, and 3) analysis of the 3D solid body. The software program used in each step is also listed in the flowchart. The first step is the data collection procedure using the EinScan-Pro scanning interface which is described in the previous section. Once a warpage experiment is completed, a scan of the veneer's warped surface is conducted, and a mesh is generated.

In the second step, the mesh is imported into a solid modeling software called Solid Edge (Siemens PLM Software 2021). The mesh is converted into a solid body using surface identification and extraction tools. In the final step, the reconstructed solid body is imported into AutoDesk Inventor (Autodesk 2021) which is a computer program that includes tools for the geometrical analysis of solid bodies. The analysis tool of interest for the warpage experiments are curvature combs. Examples of the surface visualization tools curvature comb plots employed in AutoDesk Inventor are shown in Figure 4.2.6.

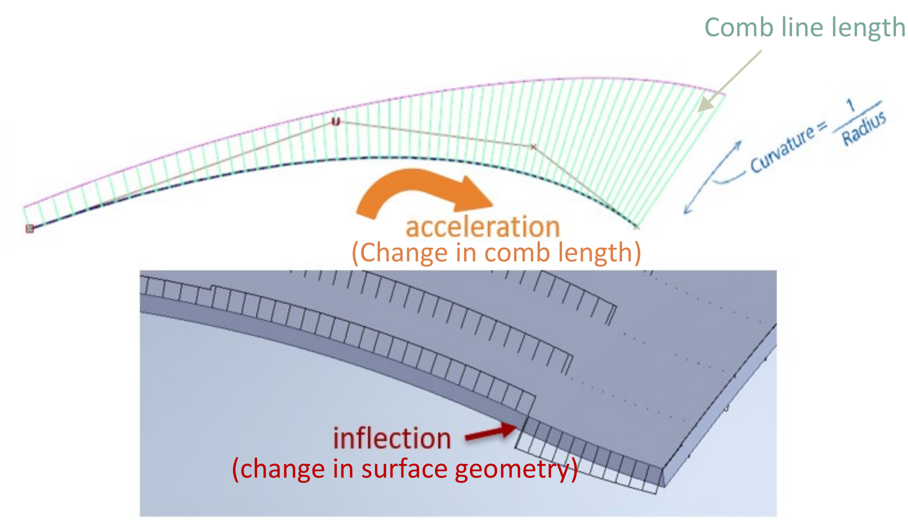

Figure 4.2.6: Examples of curvature comb plots.

Curvature combs provide a visual evaluation of the curvature of a surface. The plots are relative to each solid body, but the visualization help differentiate the warpage behavior between samples. The output curvature plot gives information about the surface based on its appearance. As demonstrated in Figure 4.2.6, the curvature's line, or comb, length equals the inverse of the curve's radius at a point. Curvature comb lines are plotted perpendicularly to the surface. A change in the lines' length represents an acceleration in the curve, indicated by the curved arrow in Figure 4.2.6. Curvature inflection, seen in the bottom image of Figure 4.2.6, is shown by the plot switching sides and demonstrates the concavity or convexity of the surface. Curvature comb analysis allows for the visualization of a warped specimens' surface geometry.

Using the surface analysis procedure developed in this section, experiments are designed to investigate the effect of different moisture gradients on warpage behavior. The two parameters of interest for manipulation are gradient magnitude and gradient area. Two different gradient magnitudes and three different sized gradient areas are used in experiments to analyze the effect of each gradient on warpage behavior. The experimental matrix in Figure 4.2.7 lists the warpage experiments that were conducted by the species and parameter manipulation used.

			Species				
			Hickory	Red oak	Yellow-poplar	Southern yellow pine	Douglas-fir
Parameter Manipulation	Gradient magnitude	low	X	X	X	X	X
		high		X	X	X	X
	Gradient area	small	X	X			X
		standard	X	X			X
		large	X	X			X

Figure 4.2.7: Experimental design matrix for warpage experiments x

The matrix represents the partial factorial design scheme for the variable to test during warpage simulations. It is used to visualize all the combinations of factor-levels that will be tested during this set of experiments. Not every parameter manipulation is applied on every species, and this is indicated by the blank spaces in the chart.

In addition to gradient magnitude and gradient area but not listed in the experimental parameter matrix, the effect of veneer thickness on warpage behavior is also investigated. Douglas-fir in three different thicknesses (0.10", 0.125" and 0.14") are used to obtain surface deformation observations. The warpage results of the thickness variable are presented in Section 4.3.1.

Using the matrix as a guide for experimental design, the outcomes of the warpage simulations are analyzed for each experimental variable's effect on warpage behavior. The three different experimental manipulations used in the warpage simulations are: thickness of the veneer specimen, concentration of the moisture gradient, and the size of the panel's surface area experiencing warpage. In the following sections, curvature comb analysis results are presented for each of the three experimental variables.

4.3 Results and Discussion

The following section presents the observations obtained from warpage experiments based on manipulating an applied moisture gradient. Results are obtained from using the procedure developed to analyze the 3D scan data collected during each experiment. Following conversion of the scan data into a solid, three-dimensional body, the surfaces of the specimens are analyzed in Autodesk Inventor using curvature comb analysis. The curvature combs are calculated from the inverse of the radius at a point, automatically generated by Inventor. The observations made from the curvature comb analysis will compare the warpage behavior of the following parameters:

- Thickness of veneers on warpage behavior
- Moisture gradient concentration manipulation
- Manipulation of moisture gradient surface area

4.3.1 Thickness of veneers on warpage behavior

The warpage experiments where thickness is the parameter under investigation are the Douglas-fir specimen experiments. In this case, two different thicknesses of Douglas-fir veneer (0.10"and 0.14" thick) are given the same moisture gradient treatment method (the low concentration gradient design). The global moisture content of the panel after treatment is calculated using the gravimetric moisture content (Equation 1). The change in global moisture content for the 0.10" sample is 1.51%, 4.21% for the 0.125" thick sample, 2.87% for the 0.14" thick Douglas-fir sample. The localized moisture content ranged from 6-27%.

The curvature comb plots from a front-on view of the Duglas-fir samples of varying thickness are shown in Figure 4.3.1.

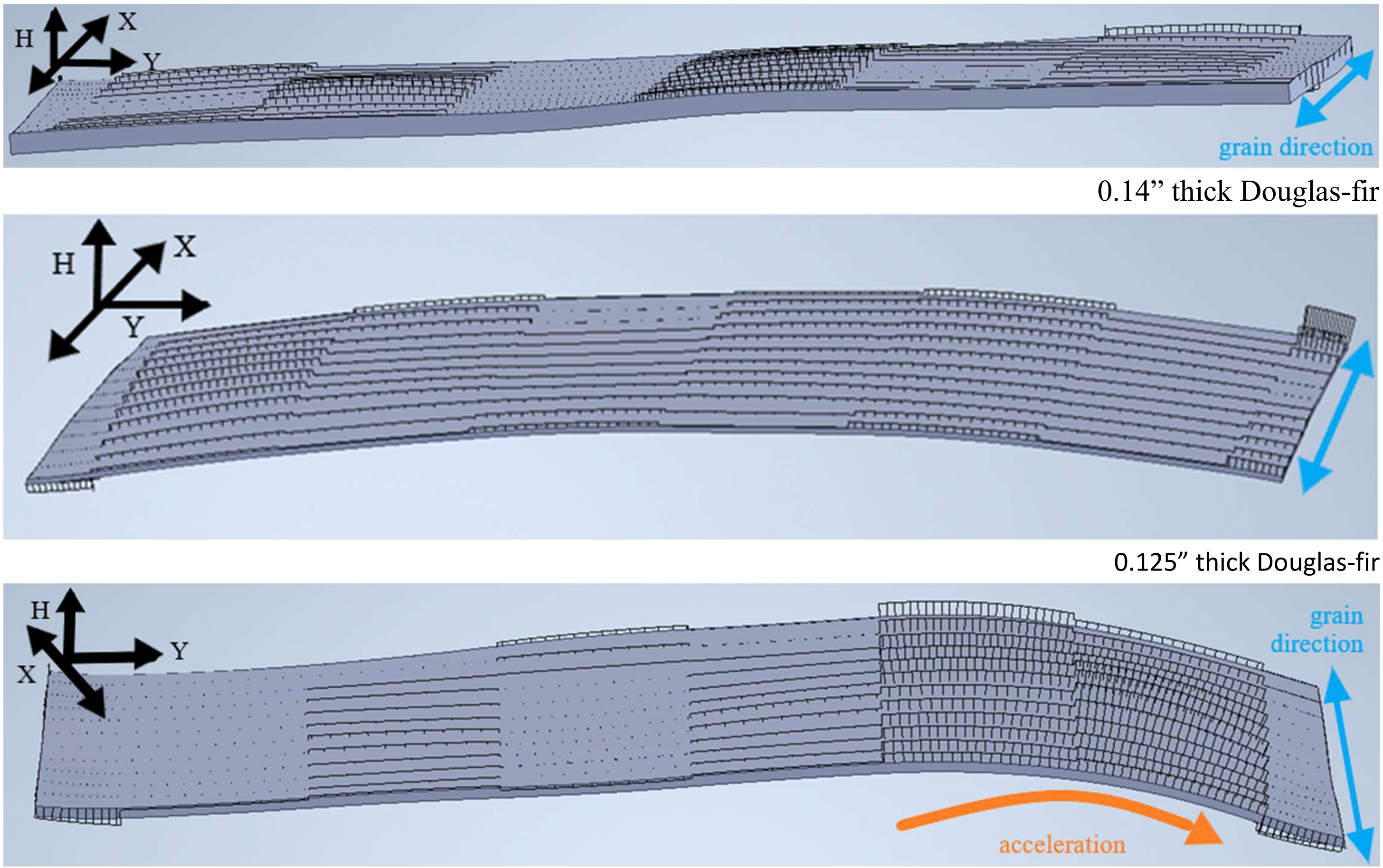

0.10” thick Douglas-fir

Figure 4.3.1: Curvature comb analysis plots of different Douglas-fir thicknesses.

As seen in Figure 4.3.1, the thinner veneer specimen experiences a greater amount of warpage. A greater magnitude of deformation on the 0.10” thick specimen is indicated by the greater acceleration comb length, highlighted by the orange arrow on the right side of the specimen when warpage is the greatest. In contrast, the 0.14” thick specimen has curvature combs of much less acceleration and length. The areas where the comb length is visible helps visualize the areas of the panel with the greatest amount of surface deformity.

4.3.2 Moisture gradient concentration manipulation

When analyzing the warpage behavior produced by the moisture gradients of different magnitudes, general conclusions can be obtained from the curvature comb plot analysis. For this example, 0.14” thick Douglas-fir veneer is used. A trial of both the low and high magnitude moisture gradients are run and the resultant curvature analysis is presented in Figure 4.3.2.

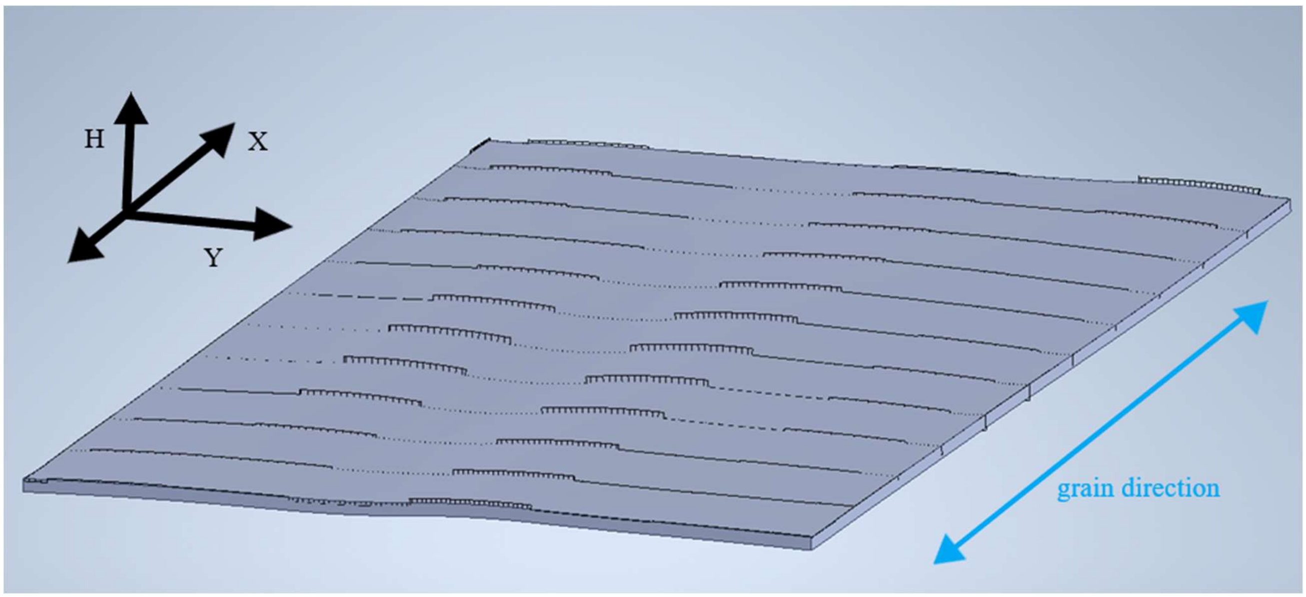

Low Magnitude Moisture Gradient

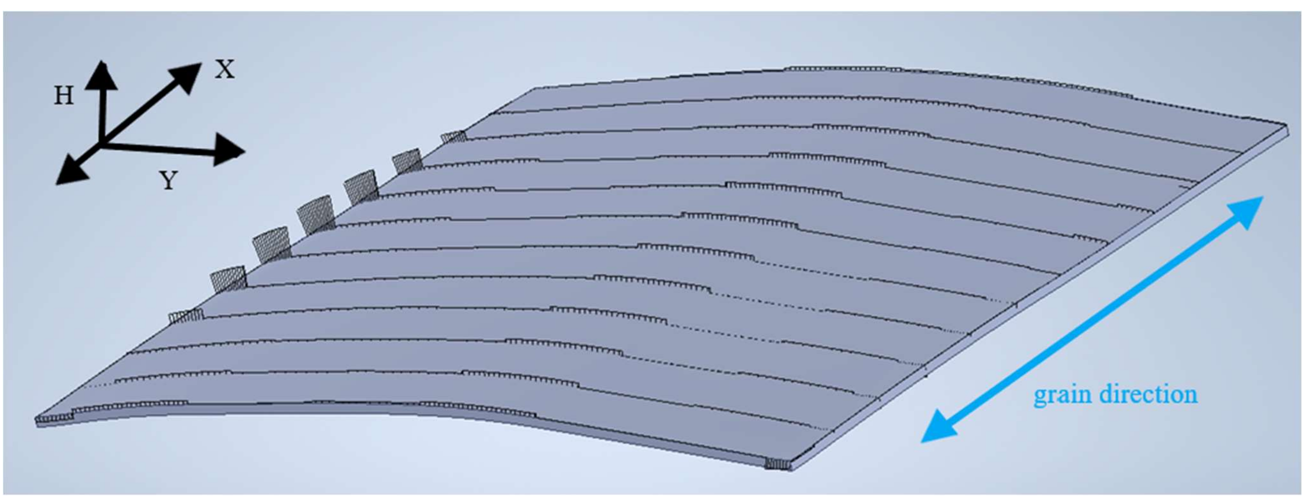

High Magnitude Moisture Gradient

Figure 4.3.2: Curvature comb plots of different moisture gradient concentrations.

After treatment, the change in moisture content for the low magnitude gradient is 2.87% and the high magnitude gradient is 3.51%. Results from warpage simulations analyzing the different moisture gradient magnitude scenarios are summarized with the examples in Figure 4.3.2. Overall, the high magnitude moisture gradient scenario produced warpage of greater magnitude than the low magnitude gradient. This is indicated on the high magnitude sample by the smoother and more consistent curvature combs across the surface. In the curvature comb analysis of the low magnitude moisture gradient scenario, the plot is more irregular with shorter combs.

Additionally, the curvature comb plot analysis of the low magnitude moisture gradient scenario points out deformities on the surface caused by the natural variability of wood. The break in the smooth curves of the panel observed in the center of the specimen throughout its long axis indicates a potential area of deformity such as earlywood/latewood differences. This deviation in the curvature comb plot helps highlight areas of irregularity in the warped specimens.

4.3.3 Manipulation of moisture gradient surface area

The last warpage simulation variable of interest is the manipulation of the size of the surface area of a panel experiencing warpage. The dimensions for the size of the moisture gradient contour areas are given in Table 3.2.2 in Section 3.2.

Each of the three specimens receive the same moisture induction treatments with only the location of the treatment application changing. After treatment, the change in moisture content from initial conditions for the small area is 2.55% and the large area is 2.06%. The change in moisture content for the regular dimensioned sample is 2.11%. The curvature comb plots for the three panels in Figure 4.4.3 are shown in Figure 4.4.4:

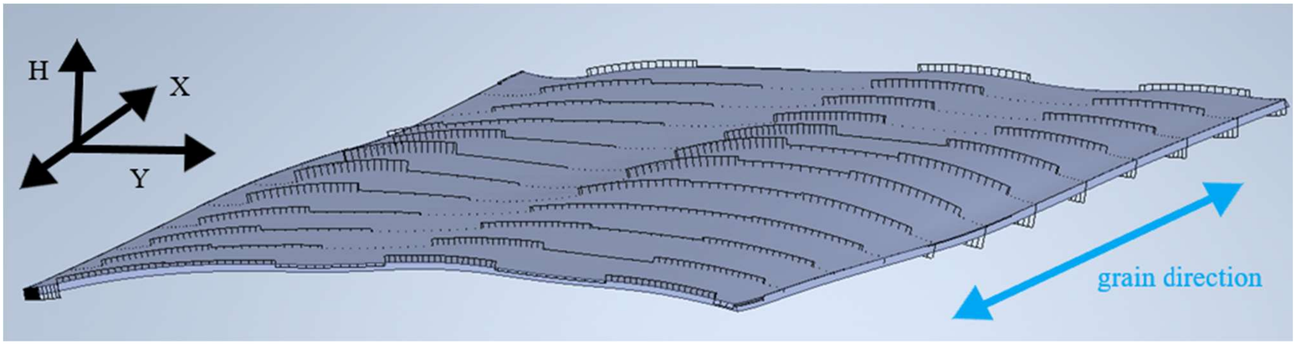

Smaller area for center warpage

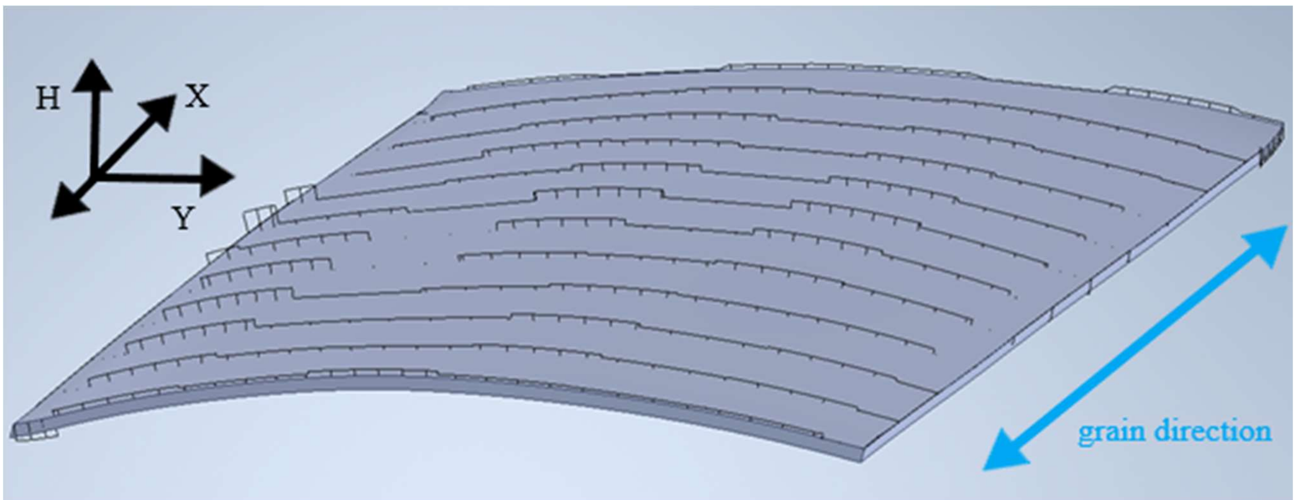

Regular area

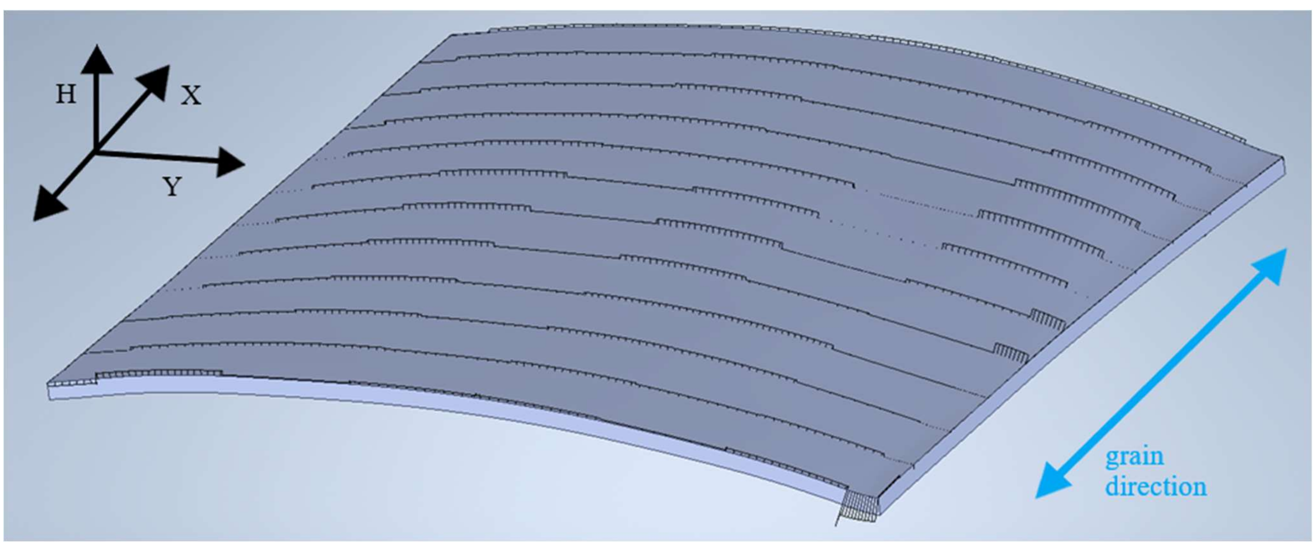

Larger area for center warpage

Figure 4.3.3: Curvature comb plots of moisture gradient area manipulation.

Manipulations in the size of a panel's surface area where moisture is applied to create a moisture gradient were the least explored variable, but some conclusions can be made from their warpage simulation experiments through curvature comb plot analysis. As seen in Figure 4.4.4, warpage behavior is different for the three different sized gradients. In the bottom plot, the specimen that received a larger amount of centralized moisture produced a smoother surface topography as indicated by the smooth and consistent curvature combs.

The specimen that incurred a smaller amount of centralized moisture, as seen in the top image of Figure 4.4.4, shows curvature comb plots of inconsistent accelerations and lengths, indicating less axisymmetric shaped warpage. The curvature comb plot behavior allows for the visualization of irregularities in the warped geometries of veneers undergoing moisture induction treatment.

The methods developed to create and measure moisture-induced warpage are presented in previous chapters. The following chapter presents the summary, conclusions, limitations, and recommendations for future work.

5.0 Summary and Conclusions

5.1 Summary

This project is inspired by theoretical models (Wood 2019), (Wood and Hanna 2020) developed to predict the warpage of anisotropic plates when exposed to moisture content changes. Moisture induction methods are developed to produce warpage of wood veneers which are considered anisotropic plates. The experimental methods developed in this project reflect the assumptions used to develop the theoretical models. Methods to induce moisture in a controlled manner are addressed by the first objective and methods to measure moisture-induced deformation are addressed in the second objective.

In the first objective, moisture induction methods are developed to create warpage of wood veneers and to quantify the amount of moisture added to a sample. Four different wetting methods are investigated to apply a known amount of moisture to the samples. Two moisture content measurement methods are investigated to measure moisture content change in the samples: 1) using an electrical resistance meter and 2) the gravimetric method for calculating moisture content (ASTM D4442). Moisture gradients of two different magnitudes are applied to the specimens and three different surface areas are investigated. The statistical significance between the two moisture gradient concentrations is determined using a paired, two-sample t-test. The results from objective one are used in objective two to study the effect of gradient magnitude and surface area on warpage.

In the second objective, a method is developed to analyze warped surface geometries and to measure moisture-induced deformation of warped veneers. A qualitative deformation monitoring system using time-lapsed photographs is used to visualize warpage using the moisture induction methods developed in objective one. A 3D structured-light scanner is used to make deformation measurements of the warped specimens. A method to analyze the 3D point cloud scan data is developed. The data analysis procedure includes creating a 3D model of the scanned data in a CAD program. Curvature comb analysis is used to observe the surface deformities of each scanned specimen. The influence on warpage of three variables is investigated. The variables are: 1) veneer thickness, 2) moisture gradient concentration, and 3) surface area of the applied gradient.

5.2 Conclusions

- Quantifiable moisture induction methods are created to experimentally induce wood warpage using parameters from the warpage prediction model described by Wood (Wood and Hanna 2020).
- Two moisture gradients of differing magnitudes are created using a combination of moisture induction methods: 1) low concentration and 2) high concentration. The gradients induce moisture concentrations of different magnitudes and are statistically significant.
- A method is developed to observe moisture-induced deformation of wood veneers using 3D scanning technology. The method uses curvature comb analysis to analyze warped surface geometries.
- Natural variability of wood affects the warped geometry of the veneer specimens. Factors such as wood anatomy, material orthotropy, and areas of high and low-density affect the shrinkage and swelling of the veneer.
- Curvature comb analysis indicates areas of surface deformities or irregular warpage behavior. This technique is used to demonstrate each variable’s effect on warpage.

- A disadvantage of the 3D scanning procedure is the inability to obtain numerical deformation data such as actual warpage elevation at various points on the sample.
- Curvature comb analysis indicates veneer thickness affects warpage behavior. Thicker veneers experience less warpage than thinner specimens.
- Curvature comb analysis indicates moisture gradient concentration affects warpage behavior. The high concentration moisture gradient produced warpage of greater magnitude than the low concentration gradient.

5.3 Limitations

- The focus of this project is to develop experimental methods to create and measure moisture-induced warpage on a limited number of samples and species. This approach demonstrates the feasibility of using the techniques. Using the developed methods, additional variables can be explored in future studies.
- Because of wood's inherent variability, validating the theoretical warpage prediction model was not attempted. The model does not account for the point-wise variability of material properties. The model can be adapted in future studies to include material property variability.
- While developing the methods to analyze the deformed geometries of the specimens undergoing warpage, the chosen technology presented the following limitations:
    - The process for converting the 3D scanner point cloud data to analyze a specimen's geometrical shape change is still under development by the 3D modeling community. Presently, the data conversion procedure is time

consuming and labor intensive. The process is not automated as multiple steps are required to build the 3D model from the 3D scan data.

5.4 Recommendations for Future Research

- Using the experimental methods developed during this project, future researchers can further explore quantifying laboratory-controlled, moisture-induced deformation.
- Increase the number of replications for warpage experiments.
- Future warpage experiments should explore the influence of material orthotropy. For example, slicing or peeling veneer along the different axes and instigating moisture-induced deformation to investigate the effect of wood orthotropy on warpage behavior.
- Multiple ply veneer specimens could be created and used under the same warpage experiments to investigate the effect a multi-ply specimen has on warpage behavior. Additional moisture induction methods may need to be developed where moisture fully penetrates the specimen to keep a consistent through-thickness moisture gradient.
- Moisture induction methods developed to create warpage can be used for the validation of the theoretical model.
- Conduct two surface scans of a specimen – before and after treatment – and run curvature comb analysis on the initial and final surface scan to compare the differences in the curvature combs.
- Three-dimensional scanning technology is a promising potential warpage monitoring method for the wood products industry. Laser interferometry technology is presently used during the quality control of manufacturing engineered wood products to monitor

moisture content. A large-scale 3D laser scanner could be installed on the line to monitor veneer flatness prior to lamination.

6.0 References

American Society for Testing and Materials (ASTM). 2020. Standard Test Methods for Direct Moisture Content Measurement of Wood and Wood-Based Materials D4442-20. West Conshohocken, Pennsylvania.

Autodesk. Autodesk Inventor. 2021. Version 25.0. San Rafael, CA.

Bodig, J. and Jayne, B. 1982. Mechanics of Wood and Wood Composites. Krieger Publishing Company; Malabar, Florida.

Cai, Z. and Dickens, J.R. 2004. Wood Composite Warping: Modeling and Simulation. *Wood and Fiber Science* 36(2): 174-185.

Cave, I.D. 1972. A Theory of the Shrinkage of Wood. *Wood Science and Technology* 6: 284-292.

Eyma, F., Méausoone, P., and Martin, P. 25 July 2003. Strains and cutting forces involved in the solid wood rotating cutting process. *Journal of Materials Processing Technology* 148: 220-225.

Grand View Research. March 2020. Wood Based Panel Market Size, Share & Trends Analysis Report. San Francisco, California, United States.

Georgopoulos, A., Ioannidia, Ch., and Valania, A. 2010. Assessing the Performance of a Structured Light Scanner. *International Archives of Photogrammetry, Remote Sensing and Spatial Information Sciences* XXXVIII(5): 250-255. Laboratory of Photogrammetry, School of Rural & Surveying Eng. National Technical University of Athens.

Gerbino, S., Del Giudice, D.M., Staiano, G., Lanzotti, A., and Martorelli, M. 21 September 2015. On the influence of scanning factors on the laser scanner-based 3D inspection process. *The International Journal of Advanced Manufacturing Technology* 84: 1787-1799.

Guo-hui, Z. 2008. Deformation Monitor Based on 3D Laser Scanner. *The International Archives of the Photogrammetry, Remote Sensing and Spatial Information Sciences*. School of Geometrics, Liaoning Technical University, Fuxin, China.

Jakieła, S., Bratasz, Ł., and Kozłowski, R. January 2008. Numerical modelling of moisture movement and related stress field in lime wood subjected to changing climate conditions. *Wood Science and Technology*

Janowiak, J.J., Hindman, D.P., and Manbeck, H.B. September 2000. Orthotropic Behavior of Lumber Composite Materials. *Wood and Fiber Science* 33(4): 580-594.

Jones, R.M. 1975. Mechanics of Composite Materials. Department of Engineering Science and Mechanics, Virginia Polytechnic Institute and State University, Blacksburg, Virginia.

Lang, E.M. 1993. Modeling the Behavior of Wood-Based Composite Sheathing Under Hygrothermal Load. Department of Wood Science and Forest Products, Virginia Polytechnic Institute and State University, Blacksburg, Virginia.

Lang, E.M., Loferski, J.R., and Dolan, J.D. March 1995. Hygroscopic deformation of wood-based composite panels. *Forest Products Journal* 45(3): 67. Forest Products Lab, Madison, Wisconsin.

Rindler, A., Vay, O., Hansmann, C., and Müller, U. 7 July 2017. Dimensional stability of multi-layered wood-based panels: a review. *Wood Science and Technology* 51: 969-996.

Sellers, T. 1985. *Plywood and Adhesive Technology*. Forest Products Utilization Laboratory. Mississippi State University Mississippi State, Mississippi.

SHINING 3D. N.d. EinScan-Pro User Manual. https://3dtechnology.ie/wp-content/uploads/2019/05/EinScan-Pro-user-manual.pdf. Accessed 14 June 2021. Xiangbin Road, Wenyan, Xiaoshan, Hangzhaou, Zhejiang, China 311258.

Shmulsky, R. and Jones, P.D. 16 May 2011. *Forest Products & Wood Science: an introduction* (6^{th} edition).

Siemens PLM Software. Solid Edge. 2021. Munich, Germany.

Suchsland, O. 2004. *The Swelling and Shrinking of Wood: A practical technology primer.* Forest Products Society, Madison, Wisconsin.

Suchsland, O., and McNatt, J.D. 1986. Computer simulation of laminated panel warping. *Forest Products Journal* 36: 16-23

Tomppo, L. May 2013. Novel Applications of Electrical Impedance and Ultrasound Methods for Wood Quality Assessment. University of Eastern Finland.

United States Department of Agriculture, U.S. Forest Service. April 2010. *Wood handbook – Wood as an engineering material.* Forest Products Laboratory, Madison, Wisconsin.

United States Department of Agriculture, U.S. Forest Service. 5 May 2021. Forest Products. https://www.fs.fed.us/research/forest-products/.

Wood, H.G. 9 May 2019. Bending and Warpage of Elastic Plates. Department of Engineering Science and Mechanics, Virginia Polytechnic Institute and State University, Blacksburg, Virginia.

Wood, H.G. and Hanna, J.A. 10 February 2021. Anisotropic swelling of anisotropic elastic panels. *Soft Matter* 17: 3137-3143.

7.0 Appendices

Appendix A: Raw Data from Warpage Experiments

Low Concentration (a1)	R.T. weight	Wet weight	O.D. weight	Average MC after Treatment	RT MC	Percent Change in MC
DFb1-E-a1	101.45	105.47	95.45	10.50	6.29	4.21
SYP1-E-a1	171.48	173.06	162.63	6.41	5.44	0.97
DFa1-E-a1	99.83	102.55	94.85	8.12	5.25	2.87
YP1-E-a1	72.43	74.08	70.15	5.60	3.25	2.35
DFc1-E-a1	134.5	136.45	129.17	5.64	4.13	1.51
H1-E-a1	91.25	93.13	89.04	4.59	2.48	2.11
O1-E-a1	74.64	77.64	71.57	8.48	4.29	4.19
H1-E-c1	88.05	90.26	86.67	4.14	1.59	2.55
H1-E-c3	92.5	94.36	90.31	4.48	2.42	2.06
DFa1-E-c3	103.03	105.37	100.78	4.55	2.23	2.32
DFa1-E-c1	103.55	105.48	101.59	3.83	1.93	1.90
O1-E-c1	73.28	76.17	70.33	8.30	4.19	4.11
O1-E-c3	76.6	79.09	73.45	7.68	4.29	3.39
DFc1-S-a1	135.19	138.49	131.01	5.71	3.19	2.52
YP1-S-a1	78.75	87.33	75.54	15.61	4.25	11.36
YP2-S-a1	79.66	85.26	75.37	13.12	5.69	7.43
SYP1-S-a1	153.59	163.28	149.63	9.12	2.65	6.48
DFb1-S-a1	104.99	105.86	102.86	2.92	2.07	0.85
O1-S-a1	73.95	75.25	72.75	3.44	1.65	1.79
			Average	**6.96**	**3.54**	**3.42**
			Standard Deviation	**3.29**	**1.42**	**2.50**
			CoV	**0.47**	**0.40**	**0.73**

High Concentration (a2)	R.T. weight	Wet weight	O.D. weight	Average MC after Treatment	RT MC	Percent Change in MC
YP1-E-a2	77.97	82.55	75.53	9.29	3.23	6.06
SYP1-E-a2	162.62	167.78	155.01	8.24	4.91	3.33
DFa1-E-a2	105.39	108.3	102.88	5.27	2.44	2.83
DFc1-E-a2	133.52	138.09	130.25	6.02	2.51	3.51
O1-E-a2	75.92	79.96	72.75	9.91	4.36	5.55
SYP1-S-a2	152.06	165.03	147.67	11.76	2.97	8.78
DFb1-S-a2	101.57	110.66	99.18	11.57	2.41	9.17
O1-S-a2	71.32	81.26	68.32	18.94	4.39	14.55
			Average	**10.13**	**3.40**	**6.72**
			Standard Deviation	**3.99**	**0.94**	**3.71**
			CoV	**0.39**	**0.28**	**0.55**

Table 7.1.1: Raw data from warpage experiments

Appendix B: T-Test Output from Excel

t-Test: Paired Two Sample for Means		
Low Concentration Moisture Gradient (a1)		
	Room Temp MC	*Post-Treatment MC*
Mean	3.54143467	6.960485475
Variance	2.128234425	11.41116544
Observations	19	19
Pearson Correlation	0.702014894	
Hypothesized Mean Difference	0	
df	18	
t Stat	-5.79220975	
P(T<=t) one-tail	8.64792E-06	
t Critical one-tail	1.734063607	
P(T<=t) two-tail	1.72958E-05	
t Critical two-tail	2.10092204	

Table 7.2.1: Excel output from running low concentration moisture gradient 2-tailed t-test.

t-Test: Paired Two Sample for Means		
High Concentration Moisture Gradient (a2)		
	Room Temp MC	*Post-Treatment MC*
Mean	3.402656408	10.12521956
Variance	1.011709841	18.17327258
Observations	8	8
Pearson Correlation	0.400053054	
Hypothesized Mean Difference	0	
df	7	
t Stat	-4.79050827	
P(T<=t) one-tail	0.000993984	
t Critical one-tail	1.894578605	
P(T<=t) two-tail	0.001987968	
t Critical two-tail	2.364624252	

Table 7.2.2: Excel output from running high concentration moisture gradient 2-tailed t-test.

t-Test: Two-Sample Assuming Unequal Variances		
Two Moisture Gradient Scenarios ΔMC		
	Low Concentration ΔMC	*High Concentration ΔMC*
Mean	3.419050805	6.722563148
Variance	6.620276807	13.78493214
Observations	19	9
Hypothesized Mean Difference	0	
df	12	
t Stat	-2.409273289	
P(T<=t) one-tail	0.016478218	
t Critical one-tail	1.782287556	
P(T<=t) two-tail	0.032956437	
t Critical two-tail	2.17881283	

Table 7.2.3: Excel output from the two-tailed, two-sample t-test assuming unequal variances amongst the two moisture gradient concentration groups. Variable one represents the average change in moisture content for the low concentration moisture gradient scenario and variable two is the average change in moisture content for the high concentration gradient.